Control Engineering Practice 163 (2025) 106400



Contents lists available at ScienceDirect

Control Engineering Practice

journal homepage: www.elsevier.com/locate/conengprac



Robust prediction-based control for unknown time-varying delays and disturbances in spherical motion platform

Seong-Min Lee [a,b,*], Sangheon Lee [c], Hungsun Son [d,**]

[a] Department of Mechanical Systems Engineering, Jeju National University, Jeju, 63243, South Korea
[b] Major of Mechatronics Engineering and faculty of Applied Energy System, Jeju National University, Jeju, 63243, South Korea
[c] School of Mechanical Engineering, Kyungpook National University, Daegu, 41566, South Korea
[d] Department of Mechanical Engineering, Ulsan National Institute of Science and Technology, Ulsan, 44919, South Korea

ARTICLE INFO

Keywords:
Lyapunov–Krasovskii functional
Prediction-based control
Preview trajectory
Unknown time-varying delay

ABSTRACT

This paper presents a new prediction-based controller utilizing enhanced preview and state prediction methods to deal with unknown time-varying delays and disturbances. In practice, uncertain and variable time delays in virtual reality applications can lead to control instability and a significant reduction in the overall sense of realism. In this paper, a robust prediction-based control (RPC) is proposed for the spherical motion platform (SMP) to compensate for the effects of the time-varying delays and disturbances. The RPC comprises a preview strategy and state/disturbance prediction methods with an estimator to handle unknown time-varying delays. In addition, a newly proposed preview method improves the system's ability to follow a time-varying reference trajectory. The stability analysis for the time-delayed system incorporating the RPC is conducted using the Lyapunov–Krasovskii approach. Numerical simulations and various experiments demonstrate that the RPC effectively leads the state to converge to the desired trajectory within an error bound under various conditions of time-varying delays in the presence of disturbances, whereas the existing controllers have limitations in reducing the desired control errors. Consequently, the results validate the feasibility and effectiveness of the RPC in real-world applications, demonstrating its robustness in handling time-varying delays through practical implementation on the SMP.

1. Introduction

Time delay has been a common but critical problem in control for transportation and mechatronic systems caused by the actuator (Ma et al., 2022), delay in the measurement chain (Gao, 2015), and network system and communication (Abolfazli et al., 2022; Liu et al., 2021; Xu, Liu et al., 2021). The unknown and uncertain time delays can significantly impact the closed-loop system, reducing bandwidth and potential instability. Time delays introduce a non-minimum phase phenomenon characterized by right-half plane zeros in a rational function. This eventually results in reducing control bandwidth and phase margin. In addition, the delay causes the system state to track the delayed reference trajectory.

Various control strategies have been explored in recent years for connected vehicles (Abolfazli et al., 2022; Liu et al., 2021), trains (Tang et al., 2018), connected cruise control (Molnár et al., 2018), autonomous vehicles (Xu, Peng et al., 2021), unmanned vehicles (Lee et al., 2023), and teleoperation (Guajardo-Benavides & Arteaga, 2023; Hernández-Ortiz & Arteaga-Pérez, 2020; Yang et al., 2019). For high-speed control of trains, robust stochastic control (Tang et al., 2018) has been developed to handle nonlinearity, parametric uncertainties, and time-varying input delays, but the controllers require prior knowledge of delays. The predictor feedback controller for the connected cruise control (Molnár et al., 2018) can robustly deal with time-varying delays, improving control stability in the presence of packet losses. However, the controllers (Molnár et al., 2018; Tang et al., 2018) do not utilize a preview method and lead to delay effects. The predictor-based controller only guarantees that the predicted future state converges to the current reference trajectory, eventually leading to convergence of the current state to the delayed reference trajectory (Lee & Son, 2022). The preview method has been implemented for autonomous vehicles (Xu, Peng et al., 2021) by compensating for constant input delay and steering lag and considering future road curvatures. A

* Corresponding author at: Department of Mechanical Systems Engineering, Jeju National University, Jeju, 63243; Major of Mechatronics Engineering and faculty of Applied Energy System, Jeju National University, Jeju, 63243, South Korea.
** Corresponding author.
E-mail addresses: leesm128@jejunu.ac.kr (S.-M. Lee), ssle8653@knu.ac.kr (S. Lee), hson@unist.ac.kr (H. Son).

https://doi.org/10.1016/j.conengprac.2025.106400
Received 23 December 2024; Received in revised form 16 March 2025; Accepted 2 May 2025
Available online 1 June 2025
0967-0661/© 2025 Published by Elsevier Ltd.

Nomenclature

χ	Predicted state vector.
χ_d	Previewed reference trajectory.
$\boldsymbol{\Theta}$, $\boldsymbol{\Phi}$	State of predictors for preview trajectory and disturbance, respectively.
ϵ	Prediction error.
$\mathbf{A}$, $\mathbf{B}$	System and input matrices.
$\mathbf{a}_d$	Acceleration of desired trajectory.
$\mathbf{d}$	External disturbance.
$\mathbf{e}$	Desired control error.
$\mathbf{e}_d$	Tracking control error.
$\mathbf{u}$	Control input vector.
$\mathbf{x}$	System state vector.
$\mathbf{x}_d$	Time-varying reference trajectory.
h	Time-varying delay.
q_0, p_0, m, r	Predictor gains.
DOF	Degree-of-Freedom.
ISS	Input-to-State Stability.
LKF	Lyapunov–Krasovskii Functional.
PC	Prediction-based Control.
PPC	Prediction-based Preview Control.
RPC	Robust Prediction-based Control.
SMP	Spherical Motion Platform.

robust predictor-based sliding mode control (Lee et al., 2023) has been developed for unmanned aerial vehicles to deal with various known and constant time delays. However, in practice, the delays are unknown and can vary over time.

The time delay problem becomes more critical in the operation of motion simulators, which are widely utilized to provide a virtual environment, with the increasing demand for virtual reality since humans are highly sensitive to small delays, which can cause simulator sickness (Moss et al., 2011). However, most existing research has focused on increasing motion range or controlling the motion simulator against disturbances and uncertainties (Lee et al., 2021). The developed spherical motion platform (SMP) (Lee et al., 2021) is capable of unlimited rotational motion but requires a wireless data link for communication between inside and outside the spherical cockpit, leading to delay problems. A prediction-based preview control (PPC) (Lee & Son, 2022) is developed to deal with only the known constant delay in the SMP. However, in real applications, the delay is unknown and varies with respect to time. Notably, there has been little exploration of delay-tolerant control for motion platforms, even though delay issues become more critical in those applications.

In order to deal with time-varying delays, several methods (Deng et al., 2021; Léchappé et al., 2018a, 2018b; Sanz et al., 2020) have been developed. The controllers can stabilize the states under the delays with also delay estimators (Deng et al., 2021; Léchappé et al., 2018a) but cannot compensate for the delay effect causing to track the delayed trajectory. Thus, the prediction-based control based on the preview method should be developed to minimize the delay effect and improve the control stability despite unknown time-varying delays.

In this paper, a robust prediction-based control (RPC) has been proposed to improve the control performance in spite of unknown and time-varying delays. The main contributions of this paper are summarized as follows:

1. The RPC is developed for spherical motion simulators to enhance virtual reality experiences, particularly time delay between visual information and motion cues that degrade operational performance causing simulator sickness. The RPC integrates delay estimation to effectively compensate for unknown time-varying input delays.
2. The RPC also comprises predictions for preview trajectory and future information of disturbance and further state prediction, improving the control performance under time-varying delays. In addition, the control stability of the closed-loop system combined with RPC and the SMP, including time-varying delays and disturbance, is proved by utilizing Lyapunov–Krasovskii functional (LKF).
3. The proposed controller is implemented to a full-scale motion platform to demonstrate the control performance in comparison with the existing prediction-based controllers. Experimental results demonstrate a significant reduction in time delay effects, leading to enhanced tracking performance even in the presence of substantial time-varying delays up to 1.5 s. This improvement contributes to a more realistic and immersive virtual environment experience.

The remainder of the paper is organized as follows. The problem is formulated, and the existing control systems are analyzed in Section 2. In order to improve the current limitations, the proposed controller RPC is developed, and the stability of the closed-loop system, including RPC, is proved in Section 3. In Sections 4 and 5, numerical simulations and experiments validate the performance of the RPC despite time-varying input delays and external disturbances, respectively, verifying the effectiveness of the proposed control for applicability in real applications. Finally, Section 6 concludes this paper.

2. Problem formulation

The dynamics, including time-varying delays and disturbances, is first analyzed for the dynamic model of the SMP. Then, the limitations of conventional prediction-based control systems are explored.

2.1. Dynamics of spherical motion platform with time-varying delay

The dynamic model for the spherical motion platform (Lee & Son, 2022; Lee et al., 2021) is represented as

$$\dot{\mathbf{x}}(t) = \mathbf{A}\mathbf{x}(t) + \mathbf{B}\left[\mathbf{u}(t - h(t)) + \mathbf{d}(t)\right], \tag{1}$$

where $\mathbf{x} = [\mathbf{x}_1^T \ \mathbf{x}_2^T]^T \in \mathbb{R}^{2n}$ $(n = 6)$ is the state vector of the dynamics (1), $\mathbf{x}_1 = [x_1 \ x_2 \ x_3 \ x_4 \ x_5 \ x_6]^T = [x \ y \ z \ \phi \ \theta \ \psi]^T$, and $\mathbf{x}_2(t) = \dot{\mathbf{x}}_1(t)$. The position (x, y, z) is represented in an inertial frame (X_I, Y_I, Z_I), and the orientation (ϕ, θ, ψ) is represented as Euler angles between the inertial and body frames (x_b, y_b, z_b). $\mathbf{u}(t - h(t)) \in \mathbb{R}^n$ is a control input with an unknown time-varying delay $h(t) \in \mathbb{R}$, and the delay eventually incurs control instability. $\mathbf{d}(t) \in \mathbb{R}^n$ represents unknown external disturbances. $\mathbf{A} \in \mathbb{R}^{2n\times 2n}$ and $\mathbf{B} \in \mathbb{R}^{2n\times n}$ are system and input matrices, respectively. The SMP consists of a cockpit sphere, four spherical wheels, and four linear actuators, where the cockpit sphere is positioned on four small spheres without mechanical linkages. The SMP can generate six-degree-of-freedom (DOF) motion, including three-DOF unlimited rotational motion, thereby providing realistic motion cues to the operator. However, motion perception may be affected by a delay between visual and motion cues due to data transmission over a wireless link. Additionally, the cockpit sphere has a large inertia exceeding 500 kg, including the operator and onboard equipment, with a diameter of 2.4 m, incurring motion delay $h(t)$ in (1). The SMP is further affected by disturbances $\mathbf{d}(t)$, which include modeling uncertainties in $\mathbf{A}$ and $\mathbf{B}$, such as uncertain gravitational forces, torques, and inertia variations due to changes in operator weight and additional installed equipment (Lee et al., 2021). Furthermore, friction and slipping uncertainties may arise in the spherical contact surface due to wear from continuous operation. The disturbance affects control stability more severely in the presence of delays, making precise motion control more challenging. In practice, the states $\mathbf{x}(t)$ are fully measurable by an

inertial measurement unit (IMU) and encoders installed on motors (Lee et al., 2021). The following assumptions are made to construct the control system.

Assumption 1. The unknown disturbance $\mathbf{d}(t)$ and $(k+1)$-times continuously differentiable $\mathbf{d}_i^{(k+1)}(t)$ are bounded as $\|\mathbf{d}(t)\| \leq D_0$ and $\|\mathbf{d}^{(k+1)}(t)\| \leq D_{k+1}, \forall t \geq 0$.

Assumption 2. The delay and its first and second derivatives are bounded for all time intervals as $0 \leq h(t) \leq \bar{h}_0$, $|\dot{h}(t)| \leq \bar{h}_1$, and $|\ddot{h}(t)| \leq \bar{h}_2, \forall t \geq 0$.

The dynamics for the reference trajectory $\mathbf{x}_d$ can be expressed as

$$\dot{\mathbf{x}}_d(t) = \mathbf{A}_d \mathbf{x}_d(t) + \mathbf{B}_d \mathbf{a}_d(t), \tag{2}$$

where $\mathbf{A}_d = \begin{bmatrix} \mathbf{0}_{n\times n} & \mathbf{I}_n \\ \mathbf{0}_{n\times n} & \mathbf{0}_{n\times n} \end{bmatrix}$, $\mathbf{B}_d = [\mathbf{0}_{n\times n}\ \mathbf{I}_n]^T$, $\mathbf{x}_d = [\mathbf{x}_{d1}^T\ \mathbf{x}_{d2}^T]^T \in \mathbb{R}^{2n}$, $\mathbf{x}_{d1} = [x_d\ y_d\ z_d\ \phi_d\ \theta_d\ \psi_d]^T$ represents the desired position and orientation, and $\mathbf{x}_{d2} = \dot{\mathbf{x}}_{d1}$ represents desired linear and angular velocities. $\mathbf{a}_d(t) \in \mathbb{R}^n$ $(n = 6)$ is an input acceleration for the desired trajectory.

Assumption 3. The acceleration input $\mathbf{a}_d(t)$ is bounded as $\|\mathbf{a}_d(t)\| \leq A_0$ since the trajectory cannot be generated to exceed the motion capability of the SMP. In addition, $\mathbf{a}_d(t)$ is $(r+1)$-times continuously differentiable, and bounded as $\|\mathbf{a}_d^{r+1}(t)\| \leq A_{r+1}, \forall t \geq 0$.

2.2. Analysis for conventional prediction-based control

Most prediction-based controllers robustly deal with disturbances under time delay but do not compensate for the delay effect with time-varying trajectories. The delay effect critically affects humans inside the motion simulator since humans perceive the delay effect and motion discrepancy, causing simulator sickness (Kim et al., 2023; Moss et al., 2011). Thus, the preview control can be applied to reduce the delay effect. Assuming the delay h is constant and known, the controller is defined as

$$\mathbf{B}\mathbf{u}(t) = -\mathbf{B}\mathbf{R}^{-1}\mathbf{B}^T\mathbf{P}\mathbf{e}_d(t) - \mathbf{B}\hat{\mathbf{d}}(t+h) + \dot{\chi}_d(t) - \mathbf{A}\chi_d(t), \tag{3}$$

$$\chi(t) = e^{\mathbf{A}h}\mathbf{x}(t) + \int_{t-h}^{t} e^{\mathbf{A}(t-s)}\mathbf{B}[\mathbf{u}(s) + \hat{\mathbf{d}}(s+h) + \boldsymbol{\varepsilon}_p(s-h)]ds \tag{4}$$

where $\mathbf{u}(t)$ is the control input of the PPC (Lee & Son, 2022); $\mathbf{e}_d(t) = \chi(t) - \chi_d(t)$ represents tracking error; $\chi(t)$, $\chi_d(t)$, and $\hat{\mathbf{d}}(t+h)$ represent the predicted future information of the state, reference trajectory, and disturbance, respectively; $\mathbf{P}$ is the solution of the algebraic Riccati equation that minimizes the linear quadratic cost function, and $\mathbf{R}$ is the design matrix; $\boldsymbol{\varepsilon}_p$ is the prediction error for the disturbance. For the PPC, the linear quadratic cost function is defined as follows: $J = \frac{1}{2}\int_{T_0}^{T_f}(\mathbf{e}_d^T(\tau)\mathbf{Q}\mathbf{e}_d(\tau) + \bar{\mathbf{u}}^T(\tau)\mathbf{R}\bar{\mathbf{u}}(\tau))d\tau + \frac{1}{2}\mathbf{e}_d^T(T_f)\mathbf{Q}\mathbf{e}_d(T_f)$, where $\mathbf{Q}$ represents the positive semidefinite matrix and the optimal control input $\bar{\mathbf{u}}(t)$ in (3) is computed to minimize J. In practice, the error bounds for convergence may increase, leading to instability when handling time-varying delays using PPC. The prediction-based state feedback controller (Léchappé et al., 2018a) enhances tracking performance under unknown time-varying delays, and the control input can be defined as follows:

$$\mathbf{u}(t) = \mathbf{K}\underbrace{\left[e^{\mathbf{A}\hat{h}(t)}\mathbf{x}(t) + \int_{t-\hat{h}(t)}^{t} e^{\mathbf{A}(t-s)}\mathbf{B}\mathbf{u}(s)ds - \mathbf{x}_d(t)\right]}_{\mathbf{e}_d(t)}, \tag{5}$$

where $\hat{h}(t)$ is the estimated delay and $\mathbf{K}$ is a control gain. $\mathbf{e}_d(t) = \mathbf{z}(t) - \mathbf{x}_d(t)$ is the tracking error, where $\mathbf{z}(t)$ and $\mathbf{x}_d(t)$ are the predicted future state and current trajectory, respectively. The dynamical system (Léchappé et al., 2018a) is only defined without disturbance, where stability and robustness against disturbance cannot be guaranteed with large steady-state error. Other research also shows similar formulations (Deng et al., 2021; Léchappé et al., 2018b).

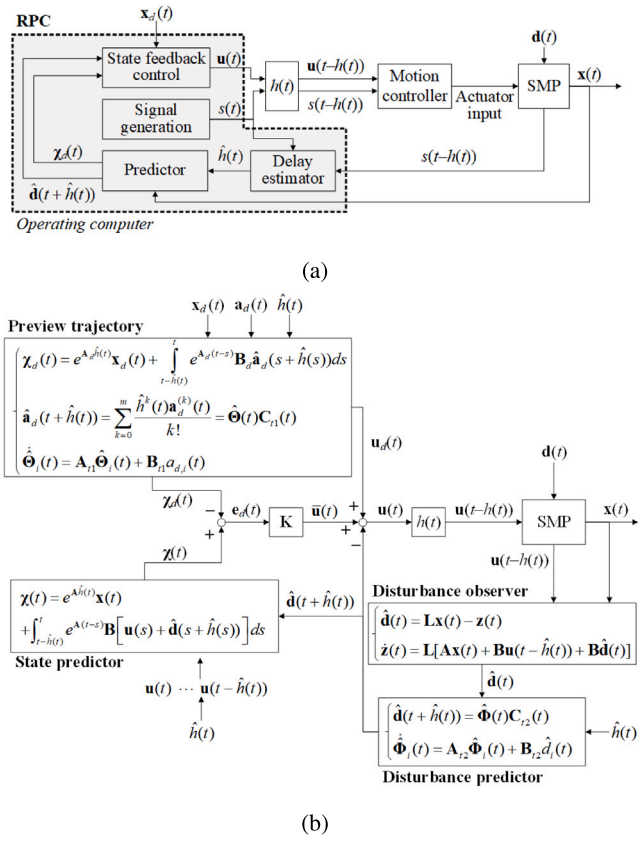


Fig. 1. Control structure of the proposed control system. (a) Control structure of RPC with delay estimation. (b) Detailed representation for RPC.

3. Robust prediction-based control

In this section, the robust prediction-based control is proposed for the spherical motion platform with a time-varying delay, as shown in Fig. 1. The controller includes three main parts: delay estimator, prediction for preview trajectory and disturbance, and preview control with state prediction.

3.1. Estimator for unknown time-varying delay

The time delay, the so-called round-trip delay, is composed of input $h_i(t)$ and output $h_o(t)$ delays, and it can be expressed as $h(t) = h_i(t - h_o(t)) + h_o(t) \approx h_i(t) + h_o(t)$ (Léchappé et al., 2018a, 2018b). It is noted that the delay $h(t)$ in (1) includes actuator, measurement, and network delays. A finite-time delay estimator (Deng et al., 2020) is introduced to estimate time-varying delay $h(t)$.

Lemma 1. *Consider a time-varying delay with Assumption 2. Define a monotonic signal as $s(t) = k_1 t$ with a positive constant k_1. The delay estimator based on the super-twisting algorithm can be defined as follows:*

$$\begin{aligned}\dot{\hat{h}}(t) &= 1 - \dot{s}^{-1}(t-\hat{h}(t))(-k_2|\sigma(t)|^{1/2}sgn(\sigma(t)) + v(t)) \\ &= 1 + k_1^{-1}k_2|\sigma(t)|^{1/2}sgn(\sigma(t)) - k_1^{-1}v(t),\end{aligned} \tag{6}$$

$$\dot{v}(t) = -k_3 sgn(\sigma(t)), \tag{7}$$

where $v \in \mathbb{R}$ is a state of the delay estimator, the sliding variable is defined as $\sigma(t) = s(t-\hat{h}(t)) - s(t-h(t)) = -k_1(\hat{h}(t)-h(t)) \in \mathbb{R}$ with positive constants k_2 and k_3. Then, the time-varying delay $h(t)$ can be estimated within finite time T_F.

Proof. See Appendix A. ■

The monotonic signal $s(t)$ for delay estimation is employed with the SMP to measure the time delay relative to a reference. The signal is generated by the operating computer, independent of the feedback controller, as shown in Fig. 1(a). Then, the signal is transmitted to the SMP through the motion controller with various delays $h(t)$ simulating communication and network latencies. The delayed signal is transmitted back to the operating computer, where the delay is computed using the estimator in (6) and (7), which utilize both the current and delayed signals. Lemma 1 verifies that the time-varying delay can be estimated within a finite time.

3.2. Prediction for preview trajectory

The time delay incurs control instability and makes the state track the delayed trajectory. The main objective of trajectory prediction is to ensure that the predicted state tracks the future reference trajectory rather than the current one, thereby minimizing the delay effect. Most existing prediction-based controllers only ensure that the predicted state converges to the current trajectory, causing the real system state to tend to the delayed trajectory without a preview trajectory (Lee & Son, 2022). Thus, the predictor in (8) is developed to predict the preview trajectory by improving existing differentiators (Lee & Son, 2022; Sanz et al., 2016) as well as to handle time-varying delays, consequently reducing delay effects. The preview trajectory can be predicted as follows:

$$\begin{cases} \chi_d(t) = e^{\mathbf{A}_d \hat{h}(t)}\mathbf{x}_d(t) + \int_{t-\hat{h}(t)}^{t} e^{\mathbf{A}_d(t-s)}\mathbf{B}_d \hat{\mathbf{a}}_d(s+\hat{h}(s))ds \\ \hat{\mathbf{a}}_d(t+\hat{h}(t)) = \sum_{k=0}^{m} \frac{\hat{h}^k(t)\mathbf{a}_d^{(k)}(t)}{k!} = \hat{\boldsymbol{\Theta}}(t)\mathbf{C}_{t1}(t) \\ \dot{\hat{\boldsymbol{\Theta}}}_i(t) = \mathbf{A}_{t1}\hat{\boldsymbol{\Theta}}_i(t) + \mathbf{B}_{t1}a_{d,i}(t) \end{cases} \tag{8}$$

with

$$\begin{aligned} \mathbf{A}_{t1} &= [-\mathbf{B}_{t1} | [\mathbf{I}_m \ \mathbf{0}_{m\times 1}]^T], \\ \mathbf{B}_{t1} &= [c_0 \ c_1 \ \cdots \ c_m]^T, \\ \mathbf{C}_{t1}(t) &= \left[1 \ \hat{h}(t) \ \cdots \ \frac{\hat{h}^m(t)}{m!}\right]^T, \\ \hat{\boldsymbol{\Theta}}(t) &= [\hat{\boldsymbol{\Theta}}_1(t) \ \hat{\boldsymbol{\Theta}}_2(t) \ \cdots \ \hat{\boldsymbol{\Theta}}_n(t)]^T, \\ \hat{\boldsymbol{\Theta}}_i(t) &= [a_{d,i}(t) \ \hat{a}_{d,i}^{(1)}(t) \ \cdots \ \hat{a}_{d,i}^{(m)}(t)]^T (i = 1, 2, \dots, n), \\ c_k &= \frac{(m+1)!}{(m-k)!(k+1)!} q_0^{k+1} (k = 0, 1, \dots, m), \end{aligned}$$

where $\chi_d(t) = \hat{\mathbf{x}}_d(t+h)$ represents the prediction for the future reference trajectory; $\mathbf{A}_{t1} \in \mathbb{R}^{(m+1)\times(m+1)}$, $\mathbf{B}_{t1} \in \mathbb{R}^{m+1}$, and $\mathbf{C}_{t1}(t) \in \mathbb{R}^{m+1}$ are system matrices of predictor for preview trajectory; $\hat{\boldsymbol{\Theta}}(t) \in \mathbb{R}^{n\times(m+1)}$ is the state of the predictor, where $\hat{\boldsymbol{\Theta}}_i(t)$ indicates the prediction of mth-order differentiation of $a_{d,i}$, $\hat{a}_{d,i}^{(m)}(t)$, m is a positive integer, and $q_0 > 0$. The future information of the input acceleration $\hat{\mathbf{a}}_d(t+\hat{h}(t))$ is first predicted using the differentiator by computing $\hat{\boldsymbol{\Theta}}$. By utilizing the predicted result $\hat{\mathbf{a}}_d(t+\hat{h}(t))$, the future reference trajectory $\chi_d(t)$ can be computed from (8). The prediction error $\boldsymbol{\varepsilon}_d(t) = \mathbf{x}_d(t+h(t)) - \chi_d(t) \in \mathbb{R}^{2n}, \forall t > T_F$ can be rewritten as

$$\boldsymbol{\varepsilon}_d(t) = \int_{t-h(t)}^{t} e^{\mathbf{A}_d(t-s)}\mathbf{B}_d\boldsymbol{\varepsilon}_q(s)ds, \tag{9}$$

where $\boldsymbol{\varepsilon}_q(t) = \mathbf{a}_d(t+h(t)) - \hat{\mathbf{a}}_d(t+h(t)) \in \mathbb{R}^n$ represents the prediction error for desired acceleration. Differentiating (9) yields the dynamics of $\boldsymbol{\varepsilon}_d(t)$ as

$$\dot{\boldsymbol{\varepsilon}}_d(t) = \mathbf{A}_d\boldsymbol{\varepsilon}_d(t) + \mathbf{B}_d\boldsymbol{\varepsilon}_q(t) - (1-\dot{h}(t))e^{\mathbf{A}_d h(t)}\mathbf{B}_d\boldsymbol{\varepsilon}_q(t-h(t)). \tag{10}$$

Lemma 2. *Consider Assumptions 2 and 3 and the predictor (8) for the preview trajectory with the prediction error dynamics of $\boldsymbol{\varepsilon}_d(t)$ in (10). Then, the error dynamics is stable, and the prediction error $\boldsymbol{\varepsilon}_d(t)$ is ultimately bounded by*

$$\lim_{t\to+\infty} \|\boldsymbol{\varepsilon}_d(t)\| \le \mu_0 \lim_{t\to+\infty} \|\boldsymbol{\varepsilon}_q(t)\| \le \mu_0\bar{\varepsilon}_q, \tag{11}$$

$$\bar{\varepsilon}_q = \sqrt{n}\left(\sum_{k=0}^{m} \frac{\bar{h}_0^k}{k!}\frac{(m+1)!q_0^{k-m-1}}{k!(m-k+1)!} + \frac{\bar{h}_0^{m+1}}{(m+1)!}\right)A_{m+1}, \tag{12}$$

where $\mu_0 = \| \int_{-\bar{h}_0}^{0} e^{\mathbf{A}_d s}ds \|$.

Proof. See Appendix B. ■

The proposed preview method can improve the control performance under time-varying delay compared to the existing preview methods (Lee & Son, 2022; Xu, Peng et al., 2021), only considering the constant time delay. Make sure that it is difficult to converge $\boldsymbol{\varepsilon}_d(t)$ and $\boldsymbol{\varepsilon}_q(t)$ to zero since the performance is affected by $\bar{h}_0$ and A_{m+1}.

3.3. RPC with state and disturbance predictions

The future state $\mathbf{x}(t+h(t))$ should be predicted since the state prediction compensates for the time delay and minimizes tracking error in order to develop the RPC. In addition, the future information of disturbance $\mathbf{d}(t+h(t))$ is predicted to improve the robustness against several disturbances in the SMP, such as uncertain inertia and gravitational torque, uncertain friction and slipping motion, and manufacturing error (Lee et al., 2021). These disturbances incur severe instability and diminish performance during control operations in the presence of time delays. Similar to Lee and Son (2022), the disturbance at current time t is first estimated as follows:

$$\begin{cases} \hat{\mathbf{d}}(t) = \mathbf{L}\mathbf{x}(t) - \mathbf{z}(t) \\ \dot{\mathbf{z}}(t) = \mathbf{L}[\mathbf{A}\mathbf{x}(t) + \mathbf{B}\mathbf{u}(t-\hat{h}(t)) + \mathbf{B}\hat{\mathbf{d}}(t)] \end{cases} \tag{13}$$

where $\mathbf{z}(t)$ is an auxiliary state, and $\mathbf{L} \in \mathbb{R}^{n\times 2n}$ is an observer gain, where $\mathbf{L} = \boldsymbol{\Lambda}(\mathbf{MB})^{\dagger}\mathbf{M}$ for a matrix $\mathbf{M}$ satisfying $\mathbf{MB}$ left-invertible and $\boldsymbol{\Lambda} = \mathrm{diag}(\lambda_1, \lambda_2, \dots, \lambda_n)$ with $\lambda_i > 0$. Then, the error dynamics of estimation error $\tilde{\mathbf{d}}(t) = \mathbf{d}(t) - \hat{\mathbf{d}}(t)$ can be obtained as

$$\begin{aligned} \dot{\tilde{\mathbf{d}}}(t) &= -\mathbf{LB}\left[\tilde{\mathbf{d}}(t) + \mathbf{u}(t-\hat{h}(t)) - \mathbf{u}(t-h(t))\right] + \dot{\mathbf{d}}(t) \\ &= -\boldsymbol{\Lambda}\tilde{\mathbf{d}}(t) + \dot{\mathbf{d}}(t), \ \forall t > T_F. \end{aligned} \tag{14}$$

In (14), the time-varying delay $h(t)$ can be estimated within T_F, and the estimation error $\tilde{\mathbf{d}}(t)$ will be eventually bounded as $\lim_{t\to+\infty} \|\tilde{\mathbf{d}}(t)\| \le \gamma_1 D_1$. Note that the disturbance is estimated regardless of the existence of the time delay. Then, the disturbance predictor for future information of disturbance $\hat{\mathbf{d}}(t+h(t))$ under time-varying delay can be utilized as

$$\begin{cases} \hat{\mathbf{d}}(t+\hat{h}(t)) = \sum_{k=0}^{r} \frac{\hat{h}^k(t)}{k!}\hat{\mathbf{d}}^{(k)}(t) = \hat{\boldsymbol{\Phi}}(t)\mathbf{C}_{t2}(t) \\ \dot{\hat{\boldsymbol{\Phi}}}_i(t) = \mathbf{A}_{t2}\hat{\boldsymbol{\Phi}}_i(t) + \mathbf{B}_{t2}\hat{d}_i(t) \end{cases} \tag{15}$$

with

$$\begin{aligned} \mathbf{A}_{t2} &= [-\mathbf{B}_{t2} \mid [\mathbf{I}_{r\times r} \ \mathbf{0}_{r\times 1}]^T] \in \mathbb{R}^{(r+1)\times(r+1)}, \\ \mathbf{B}_{t2} &= [v_0 \ v_1 \ \cdots \ v_r]^T \in \mathbb{R}^{r+1}, \\ \mathbf{C}_{t2}(t) &= \left[1 \ \hat{h}(t) \ \cdots \ \frac{\hat{h}^r(t)}{r!}\right]^T \in \mathbb{R}^{r+1}, \\ \hat{\boldsymbol{\Phi}}(t) &= [\hat{\boldsymbol{\Phi}}_1^T(t) \ \hat{\boldsymbol{\Phi}}_2^T(t) \ \cdots \hat{\boldsymbol{\Phi}}_n^T(t)]^T \in \mathbb{R}^{n\times(r+1)}, \\ \hat{\boldsymbol{\Phi}}_i(t) &= [\hat{d}_i(t) \ \hat{d}_i^{(1)}(t) \ \cdots \ \hat{d}_i^{(r)}(t)]^T (i = 1, 2, \dots, n), \\ v_k &= \frac{(r+1)!}{(r-k)!(k+1)!}p_0^{k+1} \ (k = 0, 1, \dots, r), \end{aligned}$$

where r is a positive integer and $p_0 > 0$. The prediction error can be defined as $\boldsymbol{\varepsilon}_p(t) = \mathbf{d}(t+h(t)) - \hat{\mathbf{d}}(t+\hat{h}(t)) = \tilde{\boldsymbol{\Phi}}(t)\mathbf{C}_{t2}(t) + \mathbf{R}_{t2}(t)$, where $\mathbf{R}_{t2}(t)$ is the Taylor remainder, including higher-order terms.

Lemma 3. *Consider Assumptions 1 and 2 and SMP dynamics (1). The disturbance $\hat{\mathbf{d}}(t)$ and $\hat{\mathbf{d}}(t+h(t))$ can be obtained by (13) and (15), respectively. Then, the prediction error $\boldsymbol{\varepsilon}_p(t)$ is ultimately bounded by*

$$\lim_{t\to+\infty} \|\boldsymbol{\varepsilon}_p(t)\| \le \bar{\varepsilon}_p, \tag{16}$$

$$\bar{\varepsilon}_p = \sqrt{n}\left(\sum_{k=0}^{r} \frac{\bar{h}_0^k}{k!}\frac{(r+1)!p_0^{k-r-1}}{k!(m-r+1)!} + \frac{\bar{h}_0^{r+1}}{(r+1)!}\right)D_{r+1}. \tag{17}$$

Proof. It is considered that $|d_i^{(r+1)}| \leq \|\mathbf{d}^{(r+1)}\| \leq D_{r+1}$ by Assumption 1. Similarly to the proof of Lemma 2 in Appendix B, the boundedness can be investigated as

$$\lim_{t\to+\infty} \|\boldsymbol{\varepsilon}_p(t)\| \leq \|\bar{\boldsymbol{\Phi}}(t)\mathbf{C}_{t2}(t)\| + \|\mathbf{R}_{t2}(t)\| \leq \sqrt{n}D_{r+1}\left(\sum_{k=0}^{r}\frac{\bar{h}_0^k}{k!}\frac{v_{k-1}}{v_r} + \frac{\bar{h}_0^{r+1}}{(r+1)!}\right) = \bar{\varepsilon}_p.$$

This proof is complete. ■

From the predictors for preview trajectory (8) and disturbance (15), the following state prediction strategy is proposed as

$$\chi(t) = e^{\mathbf{A}\hat{h}(t)}\mathbf{x}(t) + \int_{t-\hat{h}(t)}^{t} e^{\mathbf{A}(t-s)}\mathbf{B}\left[\mathbf{u}(s) + \hat{\mathbf{d}}(s+\hat{h}(s))\right]ds. \tag{18}$$

The future state is predicted from (18) and computed with numerical integration, incorporating the current and previous inputs $\mathbf{u}(t), \ldots, \mathbf{u}(t-\hat{h}(t))$ for practical implementation, as shown in Fig. 1(b). It is obvious that the proposed prediction can improve the robustness against time-varying delay and disturbance compared to the existing schemes (Deng et al., 2021; Léchappé et al., 2018a, 2018b; Lee et al., 2023; Lee & Son, 2022; Sanz et al., 2016, 2020). The time delay can be modeled as $h(t) = h_c + h_v(t)$, where $h_c > 0$ and $h_v(t)$ represent constant and varying delays, respectively, satisfying $h_c \gg |h_v|$ (Guajardo-Benavides & Arteaga, 2023; Hernández-Ortiz & Arteaga-Pérez, 2020). In addition, the time delay is assumed to be slowly varying since it mainly depends on communication and network delays in the SMP operation. Consequently, $h_v(t)$ can be approximated as constant during the time interval $h(t)$, resulting in $h(t)-h(t-h(t)) = h_v(t)-h_v(t-h(t)) \approx 0$. This assumption can simplify the formulation of the control system, improving practical applicability. Then, the dynamics of $\chi(t)$ can be represented as

$$\dot{\chi}(t) = \mathbf{A}\chi(t) + \mathbf{B}\left[\mathbf{u}(t) + \hat{\mathbf{d}}(t+\hat{h}(t))\right] + \boldsymbol{\varepsilon}_v(t), \tag{19}$$

where

$$\boldsymbol{\varepsilon}_v(t) = \dot{\hat{h}}(t)\mathbf{A}e^{\mathbf{A}\hat{h}(t)}\mathbf{x}(t) + e^{\mathbf{A}\hat{h}(t)}\mathbf{B}\left[\mathbf{u}(t-h(t)) + \mathbf{d}(t)\right] - (1-\dot{\hat{h}}(t))e^{\mathbf{A}\hat{h}(t)}\mathbf{B}\left[\mathbf{u}(t-\hat{h}(t)) + \hat{\mathbf{d}}(t)\right]. \tag{20}$$

In addition, the tracking error is defined as follows:

$$\mathbf{e}_d(t) = \chi(t) - \chi_d(t), \tag{21}$$

and the control input for RPC can be defined as

$$\mathbf{B}\mathbf{u}(t) = \mathbf{B}\left[\bar{\mathbf{u}}(t) - \hat{\mathbf{d}}(t+\hat{h}(t))\right] + \mathbf{u}_d(t), \tag{22}$$

where $\bar{\mathbf{u}}(t) = -\mathbf{K}\mathbf{e}_d(t)$ and $\mathbf{u}_d(t) = \dot{\chi}_d(t) - \mathbf{A}\chi_d(t)$.

Differentiating (21) and combining with (8), (19), (20), (22) result in the dynamics of $\mathbf{e}_d$ as

$$\dot{\mathbf{e}}_d(t) = \bar{\mathbf{A}}\mathbf{e}_d(t) + \boldsymbol{\varepsilon}_v(t), \tag{23}$$

where $\bar{\mathbf{A}} = [\mathbf{A}-\mathbf{B}\mathbf{K}]$ and $\mathbf{K} \in \mathbb{R}^{n\times 2n}$ is determined to make $\bar{\mathbf{A}}$ is Hurwtiz. Combining (20) with (22), then $\boldsymbol{\varepsilon}_v(t)$ is rewritten as

$$\boldsymbol{\varepsilon}_v(t) = \dot{h}(t)\mathbf{A}(\mathbf{e}_d(t) + \chi_d(t)) + e^{\mathbf{A}h(t)}\mathbf{B}\boldsymbol{\varepsilon}_p(t-h(t)) - \dot{h}(t)\mathbf{A}\int_{t-h(t)}^{t} e^{\mathbf{A}(t-s)}\left[\mathbf{B}\bar{\mathbf{u}}(s) + \mathbf{u}_d(s)\right]ds + \dot{h}(t)e^{\mathbf{A}h(t)}\left[\mathbf{B}\bar{\mathbf{u}}(t-h(t)) + \mathbf{u}_d(t-h(t))\right]. \tag{24}$$

Utilizing the following relation as $\int_{t-h(t)}^{t} e^{-\mathbf{A}s}\mathbf{u}_d(s)ds = e^{\mathbf{A}t}(\chi_d(t) - e^{\mathbf{A}h(t)}\chi_d(t-h(t)))$, (24) becomes

$$\boldsymbol{\varepsilon}_v(t) = \dot{h}(t)\mathbf{A}\mathbf{e}_d(t) - \dot{h}(t)\mathbf{A}\int_{t-h(t)}^{t} e^{\mathbf{A}(t-s)}\mathbf{B}\bar{\mathbf{u}}(s)ds + \dot{h}(t)e^{\mathbf{A}h(t)}\mathbf{B}\bar{\mathbf{u}}(t-h(t)) + e^{\mathbf{A}h(t)}\mathbf{B}\boldsymbol{\varepsilon}_p(t-h(t)) + \dot{h}(t)e^{\mathbf{A}h(t)}\dot{\chi}_d(t-h(t)). \tag{25}$$

Considering that the time delay is slowly varying and applying (10), (25) can be rewritten as

$$\boldsymbol{\varepsilon}_v(t) = \dot{h}(t)\mathbf{A}\mathbf{e}_d(t) - \dot{h}(t)\mathbf{A}\int_{t-h(t)}^{t} e^{\mathbf{A}(t-s)}\mathbf{B}\bar{\mathbf{u}}(s)ds + \dot{h}(t)e^{\mathbf{A}h(t)}\mathbf{B}\bar{\mathbf{u}}(t-h(t)) + e^{\mathbf{A}h(t)}\mathbf{B}\boldsymbol{\varepsilon}_p(t-h(t)) + \dot{h}(t)e^{\mathbf{A}h(t)}\dot{\mathbf{x}}_d(t) - \dot{h}(t)e^{\mathbf{A}h(t)}\mathbf{A}_d\boldsymbol{\varepsilon}_d(t-h(t)). \tag{26}$$

Following the Leibniz integral rule, it can be noticed that $\bar{\mathbf{u}}(t-h(t)) = \bar{\mathbf{u}}(t) - \int_{t-h(t)}^{t}\dot{\bar{\mathbf{u}}}(s)ds$, which similarly applies to $\boldsymbol{\varepsilon}_p(t-h(t))$ and $\boldsymbol{\varepsilon}_d(t-h(t))$. Then, (26) becomes

$$\boldsymbol{\varepsilon}_v(t) = \dot{h}(t)\mathbf{A}\mathbf{e}_d(t) + \dot{h}(t)e^{\mathbf{A}h(t)}\dot{\mathbf{x}}_d(t) - \dot{h}(t)\mathbf{A}\int_{t-h(t)}^{t} e^{\mathbf{A}(t-s)}\mathbf{B}\bar{\mathbf{u}}(s)ds + \dot{h}(t)e^{\mathbf{A}h(t)}\mathbf{B}\left[\bar{\mathbf{u}}(t) - \int_{t-h(t)}^{t}\dot{\bar{\mathbf{u}}}(s)ds\right] + e^{\mathbf{A}h(t)}\mathbf{B}\left[\boldsymbol{\varepsilon}_p(t) - \int_{t-h(t)}^{t}\dot{\boldsymbol{\varepsilon}}_p(s)ds\right] - \dot{h}(t)e^{\mathbf{A}h(t)}\mathbf{A}_d\left[\boldsymbol{\varepsilon}_d(t) - \int_{t-h(t)}^{t}\dot{\boldsymbol{\varepsilon}}_d(s)ds\right]. \tag{27}$$

Theorem 1. *Consider Assumptions 1–3 and the closed-loop system for SMP under time-varying delays and disturbances. In addition, the SMP tracks the time-varying reference trajectory. The proposed controller RPC (22) comprises predictors for preview trajectory (8), future state (18), and future information of disturbance (15). Then, the input-to-state stability (ISS) of the closed-loop system (23) is guaranteed by the RPC compensating for time-varying delays and disturbances. Finally, the SMP states $\mathbf{x}(t)$ can be stabilized around $\mathbf{x}_d(t)$ according to the stabilizing $\mathbf{e}_d(t)$.*

Proof. See Appendix C. ■

The maximum time delay that the RPC can handle is inherently related to the bounds. The capability to handle time delay may decrease as error bounds increase, thereby resulting in control instability. Theorem 1 proves the ISS with ultimate error boundedness, which is related to delay size and error bounds in the prediction of the future state and disturbance in Assumptions 1–3.

4. Numerical simulations

The numerical simulations validate that the proposed RPC can improve the desired tracking performance for the rotational motion of SMP despite time-varying delays and disturbances compared with PPC (Lee & Son, 2022) and PC (Deng et al., 2021). The time-varying reference trajectory for the desired orientation and angular velocity is defined as $\mathbf{x}_d(t) = [\mathbf{x}_{d1}^T(t)\ \mathbf{x}_{d2}^T(t)]^T$, where $\mathbf{x}_{d2} = \dot{\mathbf{x}}_{d1}$. The rotational dynamics (1) of the SMP is represented as

$$\begin{cases}\dot{\mathbf{x}}(t) = \begin{bmatrix}\mathbf{0}_{3\times3} & \mathbf{I}_3\\ \mathbf{0}_{3\times3} & \mathbf{0}_{3\times3}\end{bmatrix}\mathbf{x}(t) + \begin{bmatrix}\mathbf{0}_{3\times3}\\ \frac{1}{I_a}\mathbf{I}_3\end{bmatrix}[\mathbf{u}(t-h(t)) + \mathbf{d}(t)]\\ \mathbf{x} = [x_1\ x_2\ x_3\ x_4\ x_5\ x_6]^T = [\phi\ \theta\ \psi\ \dot{\phi}\ \dot{\theta}\ \dot{\psi}]^T\end{cases} \tag{28}$$

where I_a is the moment of inertia of the cockpit sphere, respectively. The unknown disturbance $\mathbf{d}(t)$ consists of uncertain dynamics and kinematics, including uncertain friction, gravitational torque, and constant disturbances in practice (Lee et al., 2021). Thus, the disturbances in the SMP are the function of the states. In the numerical simulation, the robustness of the RPC against an additionally injected constant disturbance is demonstrated. In the simulation, the time-varying input delay $h(t)$ in Table 1 satisfies the existence of upper bounds in Assumption 2 as $\bar{h}_0 = 1.5$, $\bar{h}_1 = 5e^{-2}\pi$, and $\bar{h}_2 = 5e^{-3}\pi$. The control parameters are listed in Table 1. The delay estimator (6) is utilized to estimate $\hat{h}(t)$ within a finite time as shown in Fig. 2. The delay is estimated after 1s since the delayed signal with the initial condition as $s(0) = 0.5$ can be obtained $s(t-h(t))$ after that time at least, and the estimation error converges to zero within 0.5s. Then, the future trajectory (8), disturbance (15), and state (18) can be obtained using the estimation results, thereby computing control inputs (22). Fig. 3(a) shows the comparison of prediction results of preview trajectories (χ_d) for RPC, PPC (Lee & Son, 2022), and the conventional preview method (Xu, Peng et al., 2021). The prediction performance is evaluated by the performance index using the average prediction accuracy as $e_{ss} = N^{-1}\sum_{k=1}^{N}\|\boldsymbol{\varepsilon}_d(k)\|$, where $\boldsymbol{\varepsilon}_d(k) = \mathbf{x}_d(k+h(k)) - \chi_d(k)$ represents the prediction error for the

Table 1
Parameters for numerical simulation of spherical motion platform with robust prediction-based control.

System parameters	
Mass eccentricity: $l = 0.2$ m	
Moment of inertia: $I_a = 344$ kg m^2	
Viscous friction coefficient: $C_f = 0.2$ N m s	
Time-varying delay: $h(t) = 0.5\sin(0.1\pi t) + h_c$, $(h_c = 1$ s$)$	
Disturbance: $\mathbf{d}(t) = \begin{bmatrix} 2 - C_f\dot{\phi} \\ 2 - C_f\dot{\theta} - gl\cos\theta \\ 2 - C_f\dot{\psi} \end{bmatrix}$ N m	
Reference trajectory: $\mathbf{x}_{d,1}(t) = \begin{bmatrix} 30e^{-t/20}\sin(0.1\pi t) \\ 2\sin(0.1\pi(t+10)) \\ \sin(0.2\pi t) \end{bmatrix}$ deg	
Control parameters	
DOB	$\mathbf{L} = 5[\mathbf{0}_{3\times3}\ \ \mathbf{I}_3]$
Predictor	$p_0 = 5,\ r = 1,\ q_0 = 10,\ m = 2$
Delay estimator	$k_s = 1,\ k_1 = 7,\ k_2 = 13$
State feedback control	$\mathbf{K} = 1.5[\mathbf{I}_3\ \ \mathbf{I}_3]$

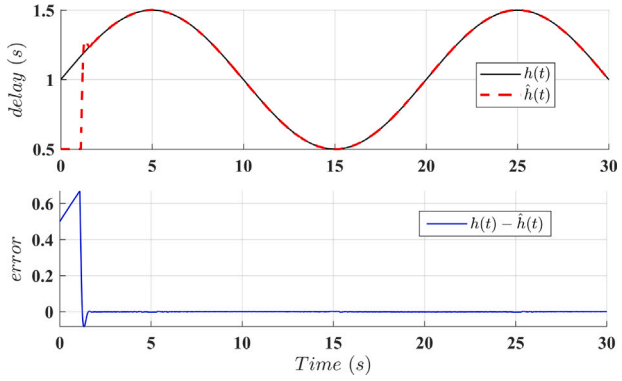


Fig. 2. Simulation results of delay estimation.

future reference trajectory and the steady-state error is calculated with the total number of data N. The RPC demonstrates significantly better prediction performance for the preview trajectory, with a prediction error of 0.37 deg, compared to the PPC and conventional preview method, which have errors of 6.44 and 7.32 deg, respectively. The RPC can more exactly predict $\hat{\mathbf{a}}_d(t+h(t))$ with delay estimation and enhanced preview method (8) in the presence of unknown time-varying delay. Similar to the preview trajectory, the prediction performance for future information of disturbance is improved by considering time-varying delay information, as shown in Fig. 3(b). Note that the prediction error for the RPC converges faster with a smaller steady-state error of 1.29 than 2.44 Nm for PPC.

Recall that the main objective of the proposed control system is to converge $\mathbf{e}_d(t) = \chi(t) - \chi_d(t)$ around zero and simultaneously make the error $\mathbf{e}(t) = \mathbf{x}(t) - \mathbf{x}_d(t)$ tend to zero as close as possible. Thus, the simulation is performed to validate the control performance and robustness of the RPC against time-varying delays and disturbances, compared with PPC (Lee & Son, 2022) and PC (Deng et al., 2021), where the control inputs for PPC and PC can be computed by (3) and (5), respectively. Fig. 4 shows the simulation results of the performance comparison. The control performance for RPC is significantly improved by the enhanced preview method and prediction for state and disturbance under time-varying delay. In contrast, the results of the PC show a much larger control error compared to the RPC and PPC due to the lack of disturbance rejection and the absence of a preview method. Moreover, the PPC does not reduce the control error due to prediction errors $\boldsymbol{\epsilon}_p(t)$ and $\boldsymbol{\epsilon}_d(t)$ caused by time-varying delays $h(t)$. The control

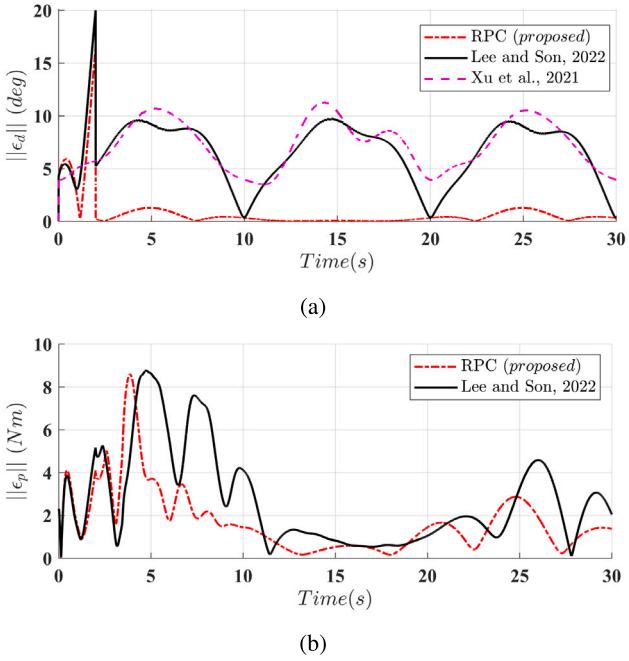


Fig. 3. Comparison of prediction performance. (a) Preview trajectory. (b) Future information of disturbance.

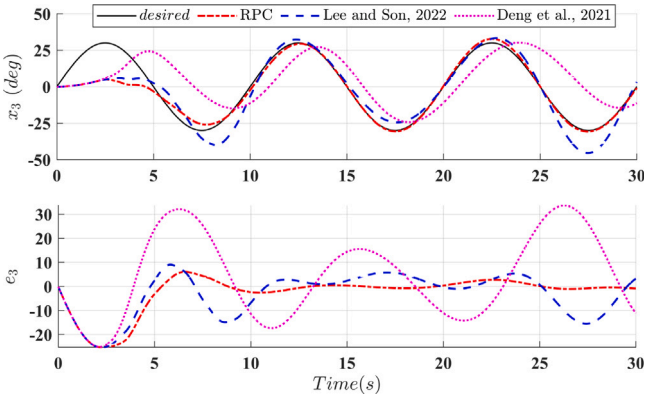


Fig. 4. Comparison of tracking control performance under time-varying delay and disturbance.

performance and robustness of the RPC against random delay have also been validated. The delay is set as $h(t) = 0.5\sin(0.1\pi)\sin(0.2\pi) - 0.1\sin(0.1\pi) + 1$s. The results demonstrate that the RPC compensates for the delay more effectively than the PPC, as shown in Fig. 5(a), where the error is evaluated by computing that $\|\mathbf{e}\| = \sqrt{e_1^2 + e_2^2 + e_3^2}$. Additionally, Fig. 5(b) verifies that the delay can be estimated within a finite time.

5. Experimental verifications

5.1. Experimental setup

The control performance and effectiveness of the RPC are verified by experiments utilizing a full-scale spherical motion platform, as shown in Fig. 6. The control performance of the RPC is compared to that of the PC (Deng et al., 2021) and PPC (Lee & Son, 2022). In the PC, the

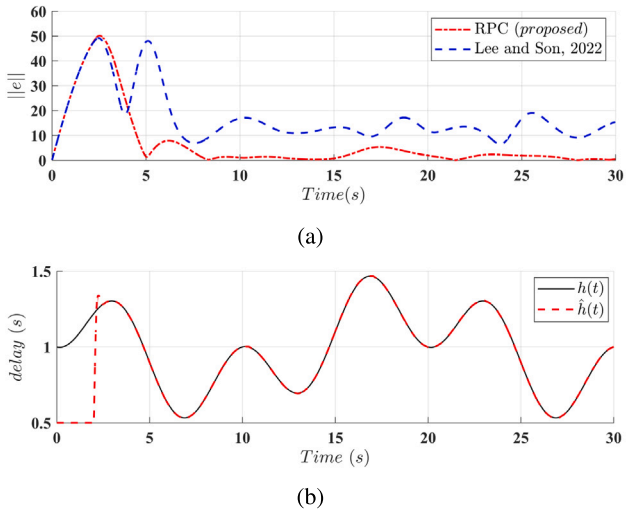


Fig. 5. Comparison of control performance for random delay. (a) Tracking control performance. (b) Delay estimation result of the RPC.

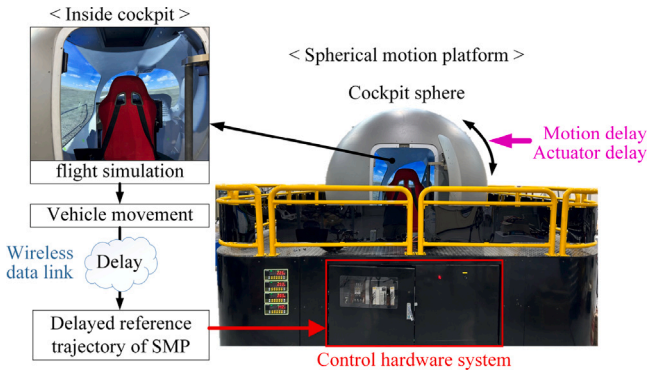


Fig. 6. Spherical motion platform with cockpit sphere.

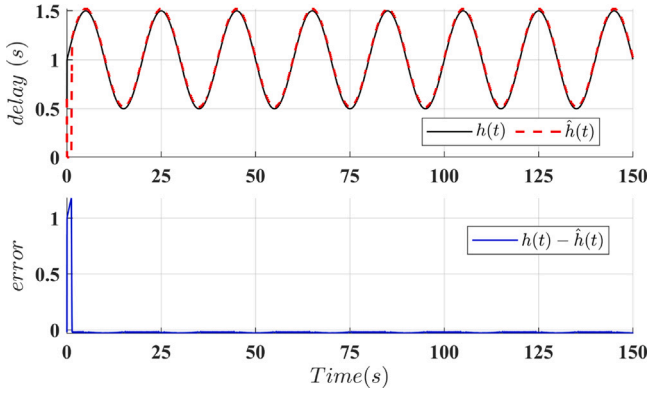


Fig. 7. Experimental result of estimation for time-varying delay.

state prediction and preview trajectory is obtained from Deng et al. (2021) and Xu, Peng et al. (2021), respectively. The SMP is used as a flight simulator, providing flight simulation to the operator inside the cockpit. The reference trajectory of the SMP is generated by the simulated flight's motion. The cockpit sphere has no mechanical linkage to the main driving system, allowing for unlimited rotation, thereby the trajectory is transmitted to the control hardware system via a wireless data link. The operator on board first perceives visual stimuli inside the cockpit, followed by motion stimuli as the cockpit rotates as closely as possible to the visual. However, the wireless data link and the large inertia of the cockpit sphere can cause time delays in both the reference trajectory and control input, including actuator delays. In addition, the SMP has several disturbance problems (Lee et al., 2021) causing control instability in the presence of the time delay. As a result, the operator may experience motion sickness due to the mismatch between visual and motion stimuli, which degrades simulation performance, as humans can perceive even small delays of about 100–300 ms (Moss et al., 2011).

5.2. Experimental results

The performance of the proposed controller RPC is compared with the existing controllers PC and PPC, where the time-varying input delay is artificially set to $h(t) = 0.5\sin(0.1\pi t)+1$s. The state is defined as $\mathbf{x}(t) = [\mathbf{x}_1^T(t)\ \mathbf{x}_2^T(t)]^T$ with an initial condition as $\mathbf{x}(0) = [\mathbf{0}_{6\times1}]$, where $\mathbf{x}_1(t) = [\phi(t)\ \theta(t)\ \psi(t)]^T$ and $\mathbf{x}_2(t) = \dot{\mathbf{x}}_1(t)$. The sinusoidal reference trajectory is set as $\mathbf{x}(t) = [\mathbf{x}_{d1}^T(t)\ \mathbf{x}_{d2}^T(t)]^T$, where $\mathbf{x}_{d1}(t) = [\phi_d(t)\ \theta_d(t)\ \psi_d(t)]^T = 10[2\sin(2\tau_d t)\quad 2\cos(2\tau_d t)\quad \sin(\tau_d t)]^T$, $\tau_d = 0.02\pi$ and $\mathbf{x}_{d2}(t) = \dot{\mathbf{x}}_{d1}(t)$. The parameters of delay estimator (6), (7) are set as $k_1 = 1$, $k_2 = 7$, and $k_3 = 13$. In addition, the control parameters for the experiments are set as follows: $\mathbf{L} = 5[\mathbf{0}_{3\times3}\ \mathbf{I}_3]$, $p_0 = 1$, $r = 1$, $q_0 = 1$, $m = 1$, and $\mathbf{K} = [1.5\mathbf{I}_3\ 0.5\mathbf{I}_3]$. The state feedback control matrix $\mathbf{K}$ is first designed by ensuring that $\bar{\mathbf{A}} = \mathbf{A} - \mathbf{BK}$ to obtain desired control performance, in the numerical simulation. Then, based on the simulation results, the matrix $\mathbf{K}$ is adjusted in experiments, considering convergence time and chattering effects caused by limited actuator performance and time delay. For the experiments, the IMU is installed inside the cockpit to measure the orientation and body angular velocity of the cockpit sphere.

5.2.1. Comparison of tracking control performance

The unknown time-varying delay is first estimated for both the PC and RPC. In contrast, for the PPC, the delay is assumed to be a constant 1s. As shown in Fig. 7, the delay is accurately estimated within a finite time, allowing the control input to be computed based on the estimation results of the time-varying delay, $\hat{h}(t)$. Fig. 8 shows the experimental results for orientation and angular velocity tracking control for the SMP utilizing the three controllers. Table 2 shows the comparison of root-mean-square-error (e_{RMS}) and maximum error (e_{MAX}) at steady-state after 10 s to evaluate the performance of the controllers. The e_{RMS} and e_{MAX} of orientation tracking control for the RPC are smaller than 1.53 and 2.85 deg, respectively. However, for the PPC and PC, the e_{RMS} (e_{MAX}) are larger than 1.73 (3.85) and 5.43 (10.45) deg, respectively. The RPC improves the orientation tracking performance larger than 10 (25) percent in e_{RMS} (e_{MAX}) compared with PPC by utilizing an enhanced prediction strategy to deal with time-varying delays. The RPC also achieves more than three times better tracking performance than the PC in both e_{RMS} and e_{MAX}. Furthermore, it should be noted that angular velocity tracking is crucial in a motion simulator since the human on board perceives rotational motions by angular velocity (Asadi et al., 2015). In fact, the orientation control in the motion simulator provides sustained linear acceleration by slowly tilting the cockpit. The e_{RMS} and e_{MAX} of angular velocity tracking control for the RPC are smaller than 0.26 and 1.19 deg, respectively. The experimental results of the RPC show more than 1.5 and about 3 times fewer tracking errors than PPC and PC, respectively, for the e_{RMS}. The proposed controller RPC can improve the operation performance to provide better virtual reality in the operation of the motion simulator with disturbance problems in the presence of time-varying delays. However, the existing controllers PC and PPC cannot compensate for the time-varying delays effectively, as shown in Fig. 8 and Table 2. It is noted that the induced delay in the visual scene and motion/actuator in Fig. 6 can be compensated by the proposed preview method (8) and prediction-based controller (22) with (15) and (18). As a result, the experimental results demonstrate that the RPC can be implemented in multi-DOF motion simulators to maximize reality by minimizing the tracking error caused by delay and disturbance.

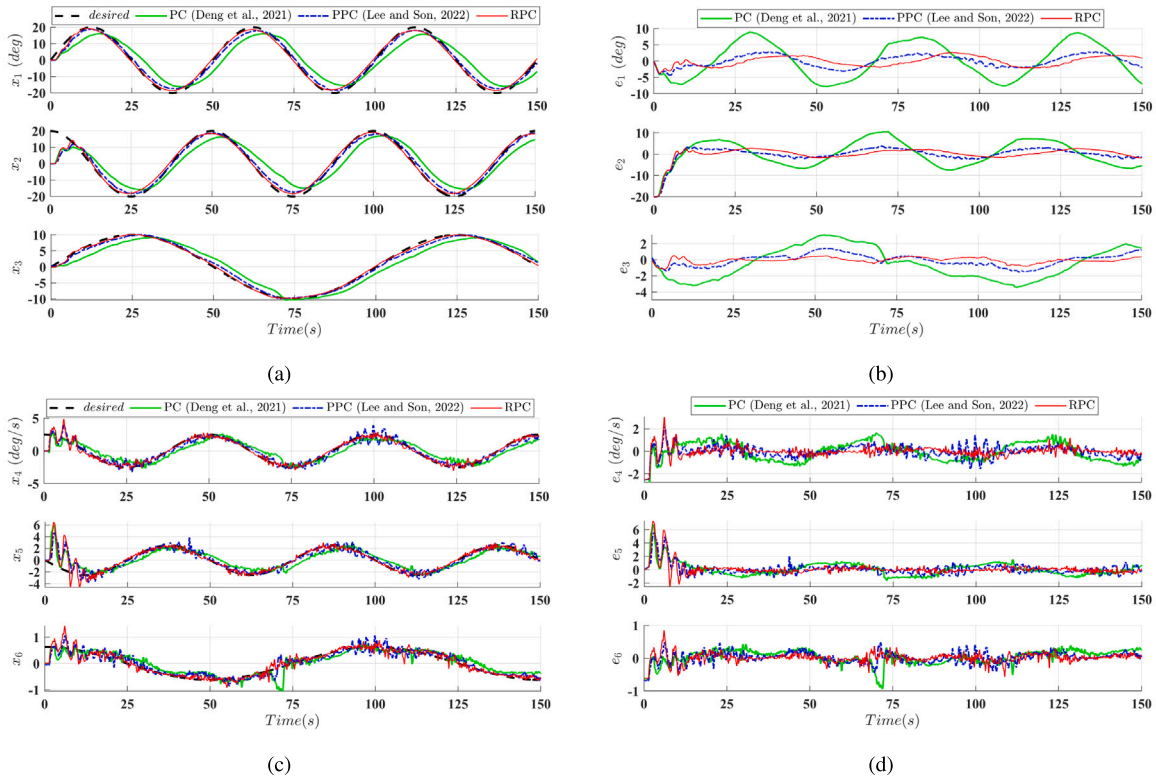


Fig. 8. Experimental results of orientation tracking control for the sinusoidal response. (a) Orientation tracking results. (b) Control error results for orientation. (c) Angular velocity tracking results. (d) Control error results for angular velocity.

Table 2
Comparison of tracking control performance.

Error		Orientation (deg)						Angular velocity (deg/s)					
		e_1		e_2		e_3		e_4		e_5		e_6	
		e_{RMS}	e_{MAX}	e_{RMS}	e_{MAX}	e_{RMS}	e_{MAX}	e_{RMS}	e_{MAX}	e_{RMS}	e_{MAX}	e_{RMS}	e_{MAX}
Controller	PC	5.49	9.06	5.43	10.54	1.91	3.43	0.78	1.63	0.74	1.63	0.21	0.94
	PPC	1.76	3.13	1.73	3.85	0.71	1.50	0.44	1.59	0.46	2.09	0.15	0.48
	RPC	1.43	2.69	1.53	2.85	0.29	0.80	0.26	1.19	0.26	1.00	0.21	0.56

5.2.2. Control performance for various time delays

The performance of the RPC is also verified by experiments including various time delays. In practice, the time delay is not constant in all cases and can vary depending on the computation load and the wireless communication environment. Six cases are experimented with increasing 0.2s in delay size for each case as $h(t) = 0.1\sin(0.1\pi t) + h_c$, where $h_c = 0.4,\ 0.6,\ 0.8,\ 1,\ 1.2,\ 1.4$s, as shown in Fig. 9(a). Fig. 9(b) and Table 3 indicate the experimental results of applying the RPC under various time delays using the SMP, verifying its effectiveness and feasibility for practical implementation. The intentionally induced time delay is estimated using a delay estimator, similar to the previous experiments. As the delay size increases, control performance degrades due to the corresponding increase in prediction errors, $\boldsymbol{\epsilon}_d(t)$ and $\boldsymbol{\epsilon}_p(t)$, which in turn increases the ultimate error bounds, $\|\mathbf{e}(\infty)\|$. In addition, the convergence time increases with the chattering effect, but control stability is still maintained despite the large delay, with $\bar{h}_0 = 1.5$ s. Consequently, the experimental results demonstrate the robustness and practical effectiveness of the RPC under various time-varying delays.

Table 3
Performance comparison of tracking control of RPC for various time-varying delays.

Delay ($h(t)$)		Orientation (deg)			Angular velocity (deg/s)		
		e_1	e_2	e_3	e_4	e_5	e_6
h_c	0.4 s	1.19	1.43	0.22	0.25	0.21	0.10
	0.6 s	1.30	1.55	0.21	0.22	0.22	0.084
	0.8 s	1.25	1.45	0.24	0.22	0.19	0.10
	1.0 s	1.20	1.33	0.36	0.28	0.22	0.11
	1.2 s	1.56	1.80	0.22	0.32	0.29	0.10
	1.4 s	1.75	1.99	0.22	0.87	0.98	0.17

The time-varying delay is set as $h(t) = 0.1\sin(0.1\pi t) + h_c$.

6. Conclusion

This paper presented the RPC, designed to handle time-varying delays and disturbances in the operation of the SMP. The enhanced state prediction and preview methods significantly improved prediction performance in the presence of time-varying delays. The ISS of the RPC was evaluated using the Lyapunov–Krasovskii approach, and its performance was validated through numerical simulations, which were compared with existing controllers. Experimental validations further demonstrated the applicability and effectiveness of the RPC in managing time-varying delays and various disturbances, compared to the existing prediction-based controllers. Furthermore, the experimental results for various time delay sizes verified the robustness of the RPC in practical implementations. Ultimately, the proposed RPC controller is expected to be widely applicable in time-delayed systems, such as transportation systems and virtual reality, including motion simulators.

The RPC can be improved to handle parametric variations, such as changes in the friction coefficient due to continuous operation in

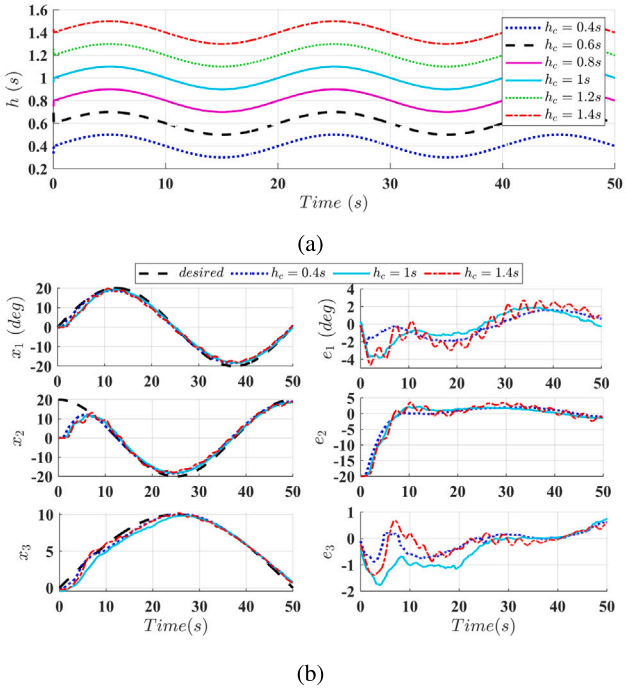


Fig. 9. Experimental results of the RPC for various time-varying delays. (a) Various time-varying delay scenarios. (b) Control results.

spherical contact within the SMP. In addition, the exact upper bound for handling the delay should be analyzed to enhance the practical applicability of the RPC. Future research will further investigate the impact of delays on stability margins to enhance the robustness of the RPC.

CRediT authorship contribution statement

Seong-Min Lee: Writing – review & editing, Writing – original draft, Visualization, Validation, Software, Formal analysis, Conceptualization. **Sangheon Lee:** Methodology. **Hungsun Son:** Writing – review & editing, Supervision, Project administration, Funding acquisition.

Declaration of competing interest

The authors declare that they have no known competing financial interests or personal relationships that could have appeared to influence the work reported in this paper.

Acknowledgments

This work was supported in part by the National Research Foundation of Korea (NRF) grant funded by the Korea government (MSIT) (No. RS-2024-00338301 and No. 2020R1A6A1A03040570), the Ministry of Trade, Industry and Energy (MOTIE) and Korea Evaluation Institute of Industrial Technology (KEIT) through the Helicopter Electric Multiple Tail Rotor Technology R&D program under Grant (RS-2022-00155776), Regional innovation mega project program through the Korea Innovation Foundation funded by Ministry of Science and ICT (2023-DD-UP-0026), and Korean Urban Air Mobility (K-UAM) Safety Operation System Core Technology Development Project with the support of the Ministry of Land, Infrastructure and Transport(MOLIT) and Korea Agency for Infrastructure Technology Advancement(KAIA) (RS-2024-00405707 and RS-2024-00404042), respectively.

Appendix A. Proof of Lemma 1

Differentiating $\sigma(t)$ and utilizing (1)–(3), the general form of the super-twisting algorithm can be obtained as follows:

$$\begin{aligned}\dot{\sigma}(t) &= -k_1\left(\dot{\hat{h}}(t) - \dot{h}(t)\right)\\ &= -k_2|\sigma(t)|^{1/2}\mathrm{sgn}(\sigma(t)) + v(t) + h_s(t),\end{aligned} \tag{29}$$

where $h_s(t) = -k_1(1-\dot{h}(t))$. In order to induce a sliding motion on $\sigma(t) = \dot{\sigma}(t) = 0$ within finite time T_F, it should be proved that $|\dot{h}_s(t)| \le \bar{h}_s$ for some finite constants (Moreno & Osorio, 2012). The boundedness of $\dot{h}_s(t)$ is simply computed as $|\dot{h}_s(t)| = k_1|\ddot{h}(t)| \le k_1\bar{h}_2 = \bar{h}_s$. Finally, the time-varying delay can be estimated exactly as $\hat{h}(t) = h(t)$ in (3) by imposing sliding motion on $\sigma(t) = \dot{\sigma}(t) = 0$ within finite time. This completes the proof.

Appendix B. Proof of Lemma 2

Consider a LKF as

$$V_0 = V_{00} + \sum_{i=1}^{3}\alpha_i V_{0i}, \tag{30}$$

where

$$\begin{aligned}V_{00} &= \boldsymbol{\epsilon}_d^T(t)\boldsymbol{\epsilon}_d(t),\\ V_{01} &= \frac{1}{n}\sum_{i=1}^{n}\tilde{\boldsymbol{\Theta}}_i^T(t)\mathbf{Q}_1\tilde{\boldsymbol{\Theta}}_i(t),\\ V_{02} &= \int_{t-\bar{h}_0}^{t}(s-t+\bar{h}_0)\|\boldsymbol{\epsilon}_q(s)\|^2 ds,\\ V_{03} &= \int_{t-\bar{h}_0}^{t}(s-t+\bar{h}_0)\|\dot{\boldsymbol{\epsilon}}_q(s)\|^2 ds,\end{aligned} \tag{31}$$

where α_i $(i = 1,2,3)$ is a positive constant. Firstly, differentiating V_{00}, it follows that

$$\begin{aligned}\dot{V}_{00} &= \boldsymbol{\epsilon}_d^T(t)(\mathbf{A}_d^T + \mathbf{A}_d)\boldsymbol{\epsilon}_d(t)\\ &\quad + \left(\mathbf{B}_d\boldsymbol{\epsilon}_q(t) - (1-\dot{h}(t))e^{\mathbf{A}_d h(t)}\mathbf{B}_d\boldsymbol{\epsilon}_q(t-h)\right)^T\boldsymbol{\epsilon}_d(t)\\ &\quad + \boldsymbol{\epsilon}_d^T(t)\left(\mathbf{B}_d\boldsymbol{\epsilon}_q(t) - (1-\dot{h}(t))e^{\mathbf{A}_d h(t)}\mathbf{B}_d\boldsymbol{\epsilon}_q(t-h)\right).\end{aligned} \tag{32}$$

In (32), following the Leibniz integral rule, it is noticed that $\boldsymbol{\epsilon}_q(t-h(t)) = \boldsymbol{\epsilon}_q(t) - \int_{t-h(t)}^{t}\dot{\boldsymbol{\epsilon}}_q(s)ds$ and $\|\mathbf{A}_d^T + \mathbf{A}_d\| = \|\mathbf{B}_d\| = 1$. Then, by using Young's inequality and combining with (9) and (10), (32) becomes

$$\begin{aligned}\dot{V}_{00} &= 2(1+\mu_1)\|\boldsymbol{\epsilon}_d(t)\|^2 + (1+\mu_1)\|\boldsymbol{\epsilon}_q(t)\|^2 + \mu_1\|\mathbf{w}_1(t)\|^2\\ &\le \mu_1\|\mathbf{w}_1(t)\|^2 + \mu_2\|\mathbf{w}_2(t)\|^2 + (1+\mu_1)\|\tilde{\boldsymbol{\Theta}}(t)\mathbf{C}_{t1}(t) + \mathbf{R}_{t1}(t)\|^2,\end{aligned} \tag{33}$$

where $\mu_1 = 1 + \bar{h}_0 + \bar{h}_1 + \bar{h}_0\bar{h}_1$, $\mu_2 = 2(1+\mu_1)(1+\bar{h}_0)$, $\|\mathbf{w}_1(t)\| = \int_{t-\bar{h}_0}^{t}\|\dot{\boldsymbol{\epsilon}}_q(s)\|ds$, and $\|\mathbf{w}_2(t)\| = \int_{t-\bar{h}_0}^{t}\|\boldsymbol{\epsilon}_q(s)\|ds$. The following relation is satisfied as $\|\tilde{\boldsymbol{\Theta}}(t)\|^2\|\mathbf{C}_{t1}(t)\|^2 \ge \mu_0\|\mathbf{R}_{t1}(t)\|^2$ with a positive constant $\mu_0 < 1$. Then, the following inequality for $\dot{V}_{00}$ is eventually obtained as follows:

$$\dot{V}_{00} \le \mu_1\|\mathbf{w}_1(t)\|^2 + \mu_2\|\mathbf{w}_2(t)\|^2 + \mu_3\|\tilde{\boldsymbol{\Theta}}(t)\|^2, \tag{34}$$

where $\mu_3 = 2(1+\mu_1)(1+1/\mu_0)\|\mathbf{C}_{t1}(t)\|^2$. Next, consider the following dynamics $\dot{\tilde{\boldsymbol{\Theta}}}_i(t) = \mathbf{A}_{t1}\tilde{\boldsymbol{\Theta}}_i(t) + [\mathbf{0}_{1\times m}\ 1]^T a_{d,i}^{(m+1)}(t)$ and there exists a positive definite matrix $\mathbf{Q}_1 \in \mathbb{R}^{(m+1)\times(m+1)}$, satisfying $\mathbf{A}_{t1}^T\mathbf{Q}_1 + \mathbf{Q}_1\mathbf{A}_{t1} = -c_{t1}\mathbf{I}_{(m+1)\times(m+1)}, \forall c_{t1} > 0$ where the matrix $\mathbf{A}_{t1}$ has a unique eigenvalue of $-q_0$ (Sanz et al., 2016). Then, the time-derivative of V_{01} applying Young's inequality can be computed as

$$\begin{aligned}\dot{V}_{01} &\le \frac{1}{n}\sum_{i=1}^{n}\left(\tilde{\boldsymbol{\Theta}}_i^T(t)(\mathbf{A}_{t1}^T\mathbf{Q}_1 + \mathbf{Q}_1\mathbf{A}_{t1})\tilde{\boldsymbol{\Theta}}_i(t)\right) + \frac{2\mu_4}{n}\sum_{i=1}^{n}\|\tilde{\boldsymbol{\Theta}}_i(t)\|\left|a_{d,i}^{(m+1)}(t)\right|\\ &\le -\frac{c_{t1}-\mu_4}{n}\sum_{i=1}^{n}\|\tilde{\boldsymbol{\Theta}}_i(t)\|^2 + \frac{\mu_4}{n}\sum_{i=1}^{n}\left|a_{d,i}^{(m+1)}(t)\right|^2\\ &\le -(c_{t1}-\mu_4)\|\tilde{\boldsymbol{\Theta}}(t)\|^2 + \mu_4 A_{m+1}^2,\end{aligned} \tag{35}$$

where $\mu_4 = \|\mathbf{Q}_1[\mathbf{0}_{1\times m}\ 1]^T\|$. In addition, differentiating V_{02} and applying for Jensen's inequality leads to

$$\dot{V}_{02} \le \bar{h}_0\|\boldsymbol{\varepsilon}_q(t)\|^2 - \frac{1}{2\bar{h}_0}\|\mathbf{w}_2(t)\|^2 - \frac{1}{2}\int_{t-\bar{h}_0}^{t}\|\boldsymbol{\varepsilon}_q(t)\|^2 ds$$
$$\le \mu_5\|\tilde{\boldsymbol{\Theta}}(t)\|^2 - \frac{1}{2\bar{h}_0}\|\mathbf{w}_2(t)\|^2 - \frac{1}{2}\int_{t-\bar{h}_0}^{t}\|\boldsymbol{\varepsilon}_q(t)\|^2 ds \tag{36}$$

where $\mu_5 = 2\bar{h}_0(1+1/\mu_0)\|\mathbf{C}_{t1}\|^2$. Similarly to (36), differentiating $V_{03}(t)$ yields to

$$\dot{V}_{03} \le \bar{h}_0\|\dot{\boldsymbol{\varepsilon}}_q(t)\|^2 - \frac{1}{2\bar{h}_0}\|\mathbf{w}_1(t)\|^2 - \frac{1}{2}\int_{t-\bar{h}_0}^{t}\|\dot{\boldsymbol{\varepsilon}}_q(t)\|^2 ds \tag{37}$$

Neglecting higher order terms ($\dot{\mathbf{C}}_{t1} \approx 0$) and fast time-varying delay ($\dot{\mathbf{R}}_{t1} \approx 0$), it is obtained that

$$\dot{\boldsymbol{\varepsilon}}_q(t) = \dot{\tilde{\boldsymbol{\Theta}}}(t)\mathbf{C}_{t1}(t) + \tilde{\boldsymbol{\Theta}}(t)\dot{\mathbf{C}}_{t1}(t) + \dot{\mathbf{R}}_{t1}(t)$$
$$= (\tilde{\boldsymbol{\Theta}}(t)\mathbf{A}_{t1}^T + [\mathbf{0}_{n\times m}\ \mathbf{a}_d^{(m+1)}(t)])\mathbf{C}_{t1}(t). \tag{38}$$

As increasing m, the following inequality is satisfied as

$$\|\dot{\boldsymbol{\varepsilon}}_q(t)\|^2 \le 2\|\mathbf{C}_{t1}(t)\|^2\left(\|\mathbf{A}_{t1}\|^2\|\tilde{\boldsymbol{\Theta}}(t)\|^2 + A_{m+1}^2\right). \tag{39}$$

Then, (37) becomes that

$$\dot{V}_{03} \le \mu_6\|\tilde{\boldsymbol{\Theta}}(t)\|^2 - \frac{1}{2\bar{h}_0}\|\mathbf{w}_1(t)\|^2 - \frac{1}{2}\int_{t-\bar{h}_0}^{t}\|\dot{\boldsymbol{\varepsilon}}_q(t)\|^2 ds + \mu_7 A_{m+1}^2, \tag{40}$$

where $\mu_6 = 2\bar{h}_0\|\mathbf{A}_{t1}\|^2\|\mathbf{C}_{t1}\|^2$ and $\mu_7 = 2\|\mathbf{C}_{t1}\|^2$. Let us consider the upper bound of $V_0(t)$ as follows:

$$V_0 \le (1+\bar{h}_0)^2\|\mathbf{w}_2(t)\|^2 + \alpha_1\|\mathbf{Q}_1\|\|\tilde{\boldsymbol{\Theta}}(t)\|^2$$
$$+ \alpha_2\bar{h}_0\int_{t-\bar{h}_0}^{t}\|\boldsymbol{\varepsilon}_q(t)\|^2 ds + \alpha_3\bar{h}_0\int_{t-\bar{h}_0}^{t}\|\dot{\boldsymbol{\varepsilon}}_q(t)\|^2 ds \tag{41}$$

Finally, the LKF $\dot{V}_0 + 2\alpha_0 V_0$ with $\alpha_0 > 0$ is upper bounded by

$$\dot{V}_0 + 2\alpha_0 V_0 \le -(\tfrac{\alpha_3}{2\bar{h}_0} - \mu_1)\|\mathbf{w}_1(t)\|^2 + (\alpha_1\mu_4 + \alpha_3\mu_7)A_{m+1}^2$$
$$- \left(\tfrac{\alpha_2}{2\bar{h}_0} - \mu_2 - 2\alpha_0(1+\bar{h}_0)^2\right)\|\mathbf{w}_2(t)\|^2$$
$$- \alpha_2\left(\tfrac{1}{2} - 2\alpha_0\bar{h}_0\right)\int_{t-\bar{h}_0}^{t}\|\boldsymbol{\varepsilon}_q(t)\|^2 ds$$
$$- \alpha_3\left(\tfrac{1}{2} - 2\alpha_0\bar{h}_0\right)\int_{t-\bar{h}_0}^{t}\|\dot{\boldsymbol{\varepsilon}}_q(t)\|^2 ds$$
$$- \left(\alpha_1 c_{t1} - \mu_3 - 2\alpha_0\alpha_1\|\mathbf{Q}_1\| - \sum_{i=1}^{3}\alpha_i\mu_{i+3}\right)\|\tilde{\boldsymbol{\Theta}}(t)\|^2 \tag{42}$$

Thus, the stability of the closed-loop system of $\boldsymbol{\varepsilon}_d(t)$ can be guaranteed from (42) for sufficiently small α_i $(i = 0,1,2,3)$ (Deng et al., 2021; Pepe & Jiang, 2006), resulting in that $\dot{V}_0 + 2\alpha_0 V_0 \le 0$. In addition, the prediction error for the future information of disturbance can be indicated as $\boldsymbol{\varepsilon}_q(t) = \tilde{\boldsymbol{\Theta}}(t)\mathbf{C}_{t1}(t) + \mathbf{R}_{t1}(t)$. The boundedness for each term in $\boldsymbol{\varepsilon}_q(t)$ can be represented as $\lim_{t\to+\infty}\|\tilde{\boldsymbol{\Theta}}_i(t)\mathbf{C}_{t1}(t)\| \le \sum_{k=0}^{m}\frac{\bar{h}_0^k}{k!}\frac{c_{k-1}}{c_m}A_{m+1}$ and $\|\mathbf{R}_{t1,i}(t)\| \le \frac{A_{m+1}\bar{h}_0^{m+1}}{(m+1)!}$ (Lee & Son, 2022). Then, one can see that

$$\lim_{t\to+\infty}\|\boldsymbol{\varepsilon}_q(t)\| \le \|\tilde{\boldsymbol{\Theta}}(t)\mathbf{C}_{t1}(t)\| + \|\mathbf{R}_{t1}(t)\|$$
$$\le \sqrt{n}A_{m+1}\left(\sum_{k=0}^{m}\frac{\bar{h}_0^k}{k!}\frac{c_{k-1}}{c_m} + \frac{\bar{h}_0^{m+1}}{(m+1)!}\right) = \bar{\varepsilon}_q.$$

Then, the following inequality holds:

$$\lim_{t\to+\infty}\|\boldsymbol{\varepsilon}_d(t)\| \le \left\|\int_{-\bar{h}_0}^{0} e^{\mathbf{A}_d s}ds\right\|\|\mathbf{B}_d\boldsymbol{\varepsilon}_q(\infty)\| \le \mu_0\bar{\varepsilon}_q. \tag{43}$$

This proof is complete.

Appendix C. Proof of Theorem 1

In order to prove ISS of (23), the LKF is firstly defined as follows:

$$V = V_1 + \sum_{i=1}^{4}\beta_i V_{i+1}, \tag{44}$$

where

$$V_1 = \mathbf{e}_d^T(t)\mathbf{P}_1\mathbf{e}_d(t),$$
$$V_2 = \int_{t-\bar{h}_0}^{t}(s-t+\bar{h})\|\bar{\mathbf{u}}(s)\|^2 ds,$$
$$V_3 = \int_{t-\bar{h}_0}^{t}(s-t+\bar{h})\|\dot{\bar{\mathbf{u}}}(s)\|^2 ds,$$
$$V_4 = \sum_{i=1}^{3}\alpha_i V_{0i} + \int_{t-\bar{h}_0}^{t}(s-t+\bar{h})\|\dot{\boldsymbol{\varepsilon}}_d(s)\|^2 ds,$$
$$V_5 = \sum_{i=1}^{n}\tilde{\boldsymbol{\Phi}}_i^T(t)\mathbf{Q}_2\tilde{\boldsymbol{\Phi}}_i(t) + \int_{t-\bar{h}_0}^{t}(s-t+\bar{h})\|\dot{\boldsymbol{\varepsilon}}_p(s)\|^2 ds. \tag{45}$$

There exists a positive definite matrix $\mathbf{P}_1 \in \mathbb{R}^{2n\times 2n}$, satisfying $\bar{\mathbf{A}}^T\mathbf{P}_1 + \mathbf{P}_1\bar{\mathbf{A}} = -c_0\mathbf{I}_{2n\times 2n}$, $\forall c_0 > 0$. Then, first, differentiating $\dot{V}_1(t)$ yields

$$\dot{V}_1 \le -c_0\|\mathbf{e}_d(t)\|^2 + \boldsymbol{\varepsilon}_v^T(t)\mathbf{P}\mathbf{e}_d(t) + \mathbf{e}_d^T(t)\mathbf{P}\boldsymbol{\varepsilon}_v(t). \tag{46}$$

Combining with (27), (46) can be rewritten as follows:

$$\dot{V}_1 \le \left(-c_0 - \eta_1 - 3\eta_2 - \eta_3 - (\bar{h}_1+2)\eta_4\right)\|\mathbf{e}_d(t)\|^2$$
$$+ \eta_2\left(\|\boldsymbol{\varepsilon}_d(t)\|^2 + \|\mathbf{v}_4(t)\|^2 + \|\dot{\mathbf{x}}_d(t)\|^2\right) + \eta_3\|\mathbf{v}_1(t)\|^2$$
$$+ \eta_4\left(\bar{h}_1\|\mathbf{v}_2(t)\|^2 + \|\boldsymbol{\varepsilon}_p(t)\|^2 + \|\mathbf{v}_3(t)\|^2\right), \tag{47}$$

where $\|\mathbf{v}_1(t)\| = \int_{t-\bar{h}_0}^{t}\|\mathbf{u}(s)\|ds$, $\|\mathbf{v}_2(t)\| = \int_{t-\bar{h}_0}^{t}\|\dot{\mathbf{u}}(s)\|ds$, $\|\mathbf{v}_3(t)\| = \int_{t-\bar{h}_0}^{t}\|\dot{\boldsymbol{\varepsilon}}_p(s)\|ds$, $\|\mathbf{v}_4(t)\| = \int_{t-\bar{h}_0}^{t}\|\dot{\boldsymbol{\varepsilon}}_d(s)\|ds$, $\eta_1 = 2\bar{h}_1\|\mathbf{P}_1\mathbf{A}\| + 2\bar{h}_1 e^{\|\mathbf{A}\|\bar{h}_0}\|\mathbf{P}_1\|\|\mathbf{B}\mathbf{K}\|$, $\eta_2 = \bar{h}_1 e^{\|\mathbf{A}\|\bar{h}_0}\|\mathbf{P}_1\|$, $\eta_3 = \eta_2\|\mathbf{A}\|\|\mathbf{B}\|$, and $\eta_4 = \eta_2\|\mathbf{B}\|$. From (9), the boundedness of $\|\boldsymbol{\varepsilon}_d(t)\|^2$ can be represented as $\|\boldsymbol{\varepsilon}_d(t)\|^2 \le e^{2\bar{h}_0}\|\mathbf{w}_1(t)\|^2$. In addition, similarly to (34), the following inequality holds: $\|\boldsymbol{\varepsilon}_p(t)\|^2 \le (1+1/\eta_0)\|\mathbf{C}_{t2}(t)\|^2\|\tilde{\boldsymbol{\Phi}}(t)\|^2$. Then, one has that

$$\dot{V}_1 \le \left(-c_0 - \eta_1 - 3\eta_2 - \eta_3 - (\bar{h}_1+2)\eta_4\right)\|\mathbf{e}_d(t)\|^2$$
$$+ \eta_2\left(e^{2\bar{h}_0}\|\mathbf{w}_1(t)\|^2 + \|\mathbf{v}_4(t)\|^2 + \|\dot{\mathbf{x}}_d(t)\|^2\right)$$
$$+ \eta_3\|\mathbf{v}_1(t)\|^2 + \eta_4\left(\bar{h}_1\|\mathbf{v}_2(t)\|^2 + \|\mathbf{v}_3(t)\|^2\right)$$
$$+ \eta_4(1+1/\eta_0)\|\mathbf{C}_{t2}(t)\|^2\|\tilde{\boldsymbol{\Phi}}(t)\|^2. \tag{48}$$

Next, similarly to (36) and (37), the following relations are obtained as follows:

$$\dot{V}_2 \le -\frac{1}{2}\int_{t-\bar{h}_0}^{t}\|\mathbf{u}(s)\|^2 ds - \frac{1}{2\bar{h}_0}\|\mathbf{v}_1(t)\|^2 + \bar{h}_0\|\mathbf{K}\|^2\|\mathbf{e}_d(t)\|^2, \tag{49}$$

$$\dot{V}_3 \le -\frac{1}{2}\int_{t-\bar{h}_0}^{t}\|\dot{\mathbf{u}}(s)\|^2 ds - \frac{1}{2\bar{h}_0}\|\mathbf{v}_2(t)\|^2 + \bar{h}_0\|\mathbf{K}\|^2\|\dot{\mathbf{e}}_d(t)\|^2. \tag{50}$$

In (50), applying (23) and (27), the following boundedness is obtained:

$$\|\dot{\mathbf{e}}_d(t)\|^2 \le \eta_5\|\mathbf{e}_d(t)\|^2 + \eta_6\|\mathbf{v}_1(t)\|^2 + \bar{h}_1^2\eta_7\|\mathbf{v}_2(t)\|^2$$
$$+ \eta_8\|\dot{\mathbf{x}}_d(t)\|^2 + \eta_7\left(\|\boldsymbol{\varepsilon}_p(t)\|^2 + \|\mathbf{v}_3(t)\|^2\right)$$
$$+ \eta_8\left(e^{2\bar{h}_0}\|\mathbf{w}_1(t)\|^2 + \|\mathbf{v}_4(t)\|^2\right), \tag{51}$$

where $\eta_5 = 8(\|\bar{\mathbf{A}}\| + \bar{h}_1\|\mathbf{A}\| + \bar{h}_1 e^{\|\mathbf{A}\|\bar{h}_0}\|\mathbf{B}\mathbf{K}\|)^2$, $\eta_6 = 8\bar{h}_1^2\|\mathbf{A}\|^2 e^{2\|\mathbf{A}\|\bar{h}_0}\|\mathbf{B}\|^2$, $\eta_7 = 8e^{2\|\mathbf{A}\|\bar{h}_0}\|\mathbf{B}\|^2$, and $\eta_8 = 8\bar{h}_1^2 e^{2\|\mathbf{A}\|\bar{h}_0}$. In addition, from (9), (10), (35), (36), and (40), one can have that

$$\dot{V}_4 \le -\left(\alpha_1 c_{t1} - \alpha_1\mu_3 - \alpha_2\mu_4 - \alpha_3\mu_5 - \alpha_4\eta_9\right)\|\tilde{\boldsymbol{\Theta}}(t)\|^2$$
$$- \frac{\alpha_2}{2}\int_{t-\bar{h}_0}^{t}\|\boldsymbol{\varepsilon}_q(s)\|^2 ds - \frac{\alpha_3}{2}\int_{t-\bar{h}_0}^{t}\|\dot{\boldsymbol{\varepsilon}}_q(s)\|^2 ds$$
$$- \frac{1}{2}\int_{t-\bar{h}_0}^{t}\|\dot{\boldsymbol{\varepsilon}}_d(s)\|^2 ds - \left(\frac{\alpha_2}{2\bar{h}_0} - \eta_{10}\right)\|\mathbf{w}_1(t)\|^2$$
$$- \left(\frac{\alpha_3}{2\bar{h}_0} - \eta_{11}\right)\|\mathbf{w}_2(t)\|^2 - \frac{1}{2\bar{h}_0}\|\mathbf{v}_4(t)\|^2 + \alpha_1\mu_3 A_{m+1}^2, \tag{52}$$

where $\eta_9 = 4\bar{h}_0(1+(1+\bar{h}_1)^2 e^{2\bar{h}_0})(1+1/\mu_0)\|\mathbf{C}_{t1}(t)\|^2$, $\eta_{10} = 4\bar{h}_0 e^{2\bar{h}_0}$, $\eta_{11} = 4\bar{h}_0(1-\bar{h}_1)^2 e^{2\bar{h}_0}$. It can be considered that there exists a positive definite matrix $\mathbf{Q}_2 \in \mathbb{R}^{(r+1)\times(r+1)}$, satisfying $\mathbf{A}_{t2}^T\mathbf{Q}_2 + \mathbf{Q}_2\mathbf{A}_{t2} = -c_{t2}\mathbf{I}_{(r+1)\times(r+1)}$, $\forall c_{t2} >$

0. Then, noting that $\dot{\boldsymbol{\varepsilon}}_p(t) = \dot{\tilde{\boldsymbol{\Phi}}}(t)\mathbf{C}_{t2}(t) = (\tilde{\boldsymbol{\Phi}}(t)\mathbf{A}_{t2}^T + [\mathbf{0}_{n\times r}\ \mathbf{d}^{(r+1)}(t)])\mathbf{C}_{t2}(t)$, similarly to (35), (36), (39), the following inequality holds:

$$\dot{V}_5 \leq -\left(c_{t2} - \eta_{12} - \eta_{13}\right)\|\tilde{\boldsymbol{\Phi}}\|^2 + \eta_{13}D_{r+1}^2 - \frac{1}{2\bar{h}_0}\|\mathbf{v}_3(t)\|^2 - \frac{1}{2}\int_{t-\bar{h}_0}^{t}\|\dot{\boldsymbol{\varepsilon}}_p(s)\|^2 ds, \tag{53}$$

where $\eta_{12} = \|\mathbf{Q}_2[\mathbf{0}_{1\times r}\ 1]^T\|/2$ and $\eta_{13} = 2\bar{h}_0(\|\mathbf{A}_{t2}(t)\|^2 + 1)\|\mathbf{C}_{t2}(t)\|^2$. It is obvious that V is upper bounded, and since from (48)–(53) it is satisfied that $\dot{V} + 2\beta_0 V \leq 0$ for sufficiently small α_i $(i = 1, 2, 3)$ and β_i $(i = 1, 2, 3, 4)$. From (23), it can be deduced that $\|\mathbf{e}_d(\infty)\| \leq \gamma_1\bar{\varepsilon}_v$ (Lee & Son, 2022), where $\bar{\varepsilon}_v = f(\bar{\varepsilon}_p, \bar{\varepsilon}_q)$ and $\bar{\varepsilon}_p$ and $\bar{\varepsilon}_q$ denote boundedness of prediction error of $\boldsymbol{\varepsilon}_p(t)$ and $\boldsymbol{\varepsilon}_q(t)$, respectively. Then, from (8), (18), (22), the ultimate boundedness can be obtained as

$$\|\mathbf{e}(\infty)\| \leq \gamma_2\|\mathbf{e}_d(\infty)\| + \gamma_3\|\boldsymbol{\varepsilon}_d(\infty)\| + \gamma_4\|\boldsymbol{\varepsilon}_p(\infty)\|, \tag{54}$$

where $\mathbf{e}(t) = \mathbf{x}(t) - \mathbf{x}_d(t)$. In (54), the tracking error $\mathbf{e}_d(t)$ can be stabilized within a bound, and then finally, the $\mathbf{x}(t)$ will track to $\mathbf{x}_d(t)$ closely with a bound if prediction error $\boldsymbol{\varepsilon}_d(t)$ and $\boldsymbol{\varepsilon}_p(t)$ are minimized. This proof is complete.

References

Abolfazli, E., Besselink, B., & Charalambous, T. (2022). On time headway selection in platoons under the MPF topology in the presence of communication delays. *IEEE Transactions on Intelligent Transportation Systems*, *23*(7), 8881–8894.

Asadi, H., Mohamed, S., & Nahavandi, S. (2015). Incorporating human perception with the motion washout filter using fuzzy logic control. *IEEE/ASME Transactions on Mechatronics*, *20*(6), 3276–3284.

Deng, Y., Léchappé, V., Moulay, E., & Plestan, F. (2021). Predictor-based control of LTI remote systems with estimated time-varying delays. *IEEE Control Systems Letters*, *5*(1), 289–294.

Deng, Y., Léchappé, V., Rouquet, S., Moulay, E., & Plestan, F. (2020). Super-twisting algorithm-based time-varying delay estimation with external signal. *IEEE Transactions on Industrial Electronics*, *67*(12), 10663–10671.

Gao, Z. (2015). Estimation and compensation for lipschitz nonlinear discrete-time systems subjected to unknown measurement delays. *IEEE Transactions on Industrial Electronics*, *62*(9), 5950–5961.

Guajardo-Benavides, E. J., & Arteaga, M. A. (2023). On the finite time force estimation for bilateral teleoperation of robot manipulators with time varying delays. *Control Engineering Practice*, *138*, Article 105622.

Hernández-Ortiz, Ó., & Arteaga-Pérez, M. A. (2020). A simple approach for the force control of bilateral teleoperated manipulators with variable time delays. *Control Engineering Practice*, *102*, Article 104564.

Kim, J., Lee, S.-M., Son, H., & Park, T. (2023). Effects of unlimited angular motion cue and cue discrepancy on simulator sickness. *Expert Systems with Applications*, *213*, Article 119196.

Léchappé, V., Moulay, E., & Plestan, F. (2018a). Prediction-based control for LTI systems with uncertain time-varying delays and partial state knowledge. *International Journal of Control*, *91*(6), 1403–1414.

Léchappé, V., Moulay, E., & Plestan, F. (2018b). Prediction-based control of LTI systems with input and output time-varying delays. *Systems & Control Letters*, *112*, 24–30.

Lee, S.-M., Shin, M., & Son, H. (2023). Robust predictor-based control for multirotor UAV with various time delays. *IEEE Transactions on Industrial Electronics*, *70*(8), 8151–8162.

Lee, S.-M., & Son, H. (2022). Prediction-based preview control of motion platform with time delay. *IEEE Transactions on Intelligent Transportation Systems*, *23*(12), 23346–23357.

Lee, S.-M., Xia, K., & Son, H. (2021). Robust tracking control of spherical motion platform for virtual reality. *IEEE Transactions on Industrial Electronics*, *68*(1), 892–901.

Liu, Y., Gao, H., Zhai, C., & Xie, W. (2021). Internal stability and string stability of connected vehicle systems with time delays. *IEEE Transactions on Intelligent Transportation Systems*, *22*(10), 6162–6174.

Ma, Y., He, X., Zhang, S., Sun, Y., & Fu, Q. (2022). Adaptive compensation for infinite number of actuator faults and time-varying delay of a flexible manipulator system. *IEEE Transactions on Industrial Electronics*, *69*(12), 13141–13150.

Molnár, T. G., Qin, W. B., Insperger, T., & Orosz, G. (2018). Application of predictor feedback to compensate time delays in connected cruise control. *IEEE Transactions on Intelligent Transportation Systems*, *19*(2), 545–559.

Moreno, J. A., & Osorio, M. (2012). Strict Lyapunov functions for the super-twisting algorithm. *IEEE Transactions on Automatic Control*, *57*(4), 1035–1040.

Moss, J. D., Austin, J., Salley, J., Coats, J., Williams, K., & Muth, E. R. (2011). The effects of display delay on simulator sickness. *Displays*, *32*(4), 159–168.

Pepe, P., & Jiang, Z.-P. (2006). A Lyapunov–Krasovskii methodology for ISS and iISS of time-delay systems. *Systems & Control Letters*, *55*, 1006–1014.

Sanz, R., García, P., & Albertos, P. (2016). Enhanced disturbance rejection for a predictor-based control of lti systems with input delay. *Automatica*, *72*, 205–208.

Sanz, R., García, P., Fridman, E., & Albertos, P. (2020). Robust predictive extended state observer for a class of nonlinear systems with time-varying input delay. *International Journal of Control*, *93*(2), 217–225.

Tang, H., Wang, Q., & Feng, X. (2018). Robust stochastic control for high-speed trains with nonlinearity, parametric uncertainty, and multiple time-varying delays. *IEEE Transactions on Intelligent Transportation Systems*, *19*(4), 1027–1037.

Xu, X., Liu, Z., Wang, F., Xie, J., & Su, P. (2021). Trajectory tracking control based on the dual-motor autonomous steering system with time-varying network-induced time delay. *Control Engineering Practice*, *116*, Article 104915.

Xu, S., Peng, H., & Tang, Y. (2021). Preview path tracking control with delay compensation for autonomous vehicles. *IEEE Transactions on Intelligent Transportation Systems*, *22*(5), 2979–2989.

Yang, H., Liu, L., & Wang, Y. (2019). Observer-based sliding mode control for bilateral teleoperation with time-varying delays. *Control Engineering Practice*, *91*, Article 104097.